



1

2 **Ocean alkalinity enhancement approaches and the predictability of**  
3 **runaway precipitation processes -**  
4 **Results of an experimental study to determine critical alkalinity ranges for safe and sustainable application scenarios**

5  
6 **Niels Suitner<sup>1</sup>, Giulia Faucher<sup>2</sup>, Carl Lim<sup>3</sup>, Julieta Schneider<sup>2</sup>, Charly A. Moras<sup>4</sup>, Ulf Riebesell<sup>2</sup> and Jens Hartmann<sup>1</sup>**

7  
8 <sup>1</sup>Institute for Geology, Universität Hamburg, Bundesstrasse 55, 20146 Hamburg, Germany

9 <sup>2</sup>GEOMAR Helmholtz Centre for Ocean Research Kiel, Wischhofstrasse 1-3, 24148 Kiel, Germany

10 <sup>3</sup>KU Leuven, Bruges, Department of Materials Engineering, B-8200, Belgium

11 <sup>4</sup>Faculty of Science and Engineering, Southern Cross University, Lismore, NSW 2480, Australia

12  
13 Correspondence: Niels Suitner (niels.suitner@uni-hamburg.de), Jens Hartmann (geo@hattes.de)

14  
15 **Orcid:**

16  
17 Niels Suitner: <https://orcid.org/0000-0003-3413-857X>

18 Giulia Faucher: <https://orcid.org/0000-0001-8930-477X>

19 Carl Lim: <https://orcid.org/0000-0002-9035-4771>

20 Julieta Schneider: <https://orcid.org/0000-0002-7271-717X>

21 Charly A. Moras: <https://orcid.org/0000-0001-6819-6167>

22 Ulf Riebesell: <https://orcid.org/0000-0002-9442-452X>

23 Jens Hartmann: <https://orcid.org/0000-0003-1878-9321>



24 **Abstract**

25

26 To ensure the safe and efficient application of Ocean Alkalinity Enhancement (OAE), it is crucial to investigate its impacts on  
27 the carbonate system. While various modeling studies showed promising results in the past, there has been a lack of empirical  
28 data to support the applicability of this technology in natural environments. Recent studies have described the effect of runaway  
29 precipitation in the context of OAE, showing that calcium carbonate formation was triggered if certain  $\Omega_{\text{aragonite}}$  saturation  
30 threshold levels were exceeded. This precipitation can adversely affect the carbon storage capacity and may in some cases  
31 result in CO<sub>2</sub> emissions. Experiments at the Espeland Marine Biological Station (Bergen, Norway) were conducted to  
32 systematically study the chemical consequences of OAE deployment. The experiments lasted for 20-25 days to monitor the  
33 temporal development of carbonate chemistry parameters after alkalinity addition and the eventually triggered carbonate  
34 precipitation process. Identified uniform patterns before and during the triggered runaway process can be described by  
35 empirical functional relationships. For the CO<sub>2</sub>-equilibrated approaches, total alkalinity levels (TA) of up to 6500  $\mu\text{eq kgsw}^{-1}$   
36 remained stable without loss of total alkalinity (TA) for up to 20 days. Higher implemented TA levels, up to 11200  $\mu\text{eq kgsw}^{-1}$ ,  
37 triggered runaway carbonate formation. Once triggered, the loss of alkalinity continued until  $\Omega_{\text{aragonite}}$  values leveled out at 5.8-  
38 6.0, resulting still in a net gain of 3600-4850  $\mu\text{eq kgsw}^{-1}$  in TA. The CO<sub>2</sub>-non-equilibrated approaches, however, remained  
39 only stable for TA additions of up to 1000  $\mu\text{eq kgsw}^{-1}$ . The systematic behavior of treatments exceeding this level allows to  
40 predict the duration of transient stability and the quantity of TA loss after this period. Once triggered, the TA-loss continued  
41 in the CO<sub>2</sub>-non-equilibrated approaches until  $\Omega_{\text{aragonite}}$  values of 2.5–5.0 were reached, in this case resulting in a net loss of TA.  
42 To prevent a net loss of TA, treated water must be diluted below the time-dependent critical levels of TA and  $\Omega_{\text{aragonite}}$  within  
43 the identified transient stability duration. Identified stability and loss patterns of added TA depend on local environmental  
44 conditions impacting the carbonate system, like salinity, temperature, biological activity, and particle abundance.  
45 Implementation of such identified stability and loss patterns into ocean biogeochemical models, capable of resolving mixing  
46 patterns of treated and untreated water parcels, would allow to predict, from the geochemical perspective, safe local application  
47 levels of TA, as well as the fate of added alkalinity, and therefore a more realistic carbon storage potential as if neglecting  
48 observed carbonate system response to OAE.



## 49 **1 Introduction**

50

51 At the current greenhouse gas emission rates, global warming well below 2°C, compared to pre-industrial levels, as targeted  
52 by the Paris Agreement (UNFCCC, 2015) might not be achievable (Meinshausen et al., 2009; Rogelj et al., 2016). To prevent  
53 such a development, international efforts have turned the spotlight on reducing greenhouse gas emissions globally. However,  
54 to comply with the climate goals, greater attention needs to be paid to carbon dioxide removal (CDR) technologies. One such  
55 marine-based technology is ocean alkalinity enhancement (OAE), a strategy that aims to chemically sequester carbon dioxide  
56 (CO<sub>2</sub>) as carbonate (CO<sub>3</sub><sup>2-</sup>) or bicarbonate (HCO<sub>3</sub><sup>-</sup>) ions in ocean water (Kheshgi, 1995; NASEM, 2022). The concept of OAE  
57 strives to increase the inorganic carbon storage capacity by increasing the total alkalinity (TA) of seawater (Caldeira & Rau,  
58 2000; Hartmann et al., 2013; Köhler et al., 2010; Schuiling & Krijgsman, 2006). Given the residence time of inorganic carbon  
59 in the ocean, it could be potentially stored for 10,000 to 100,000 years (Berner et al., 1983; Mackenzie & Garrels, 1966). An  
60 accompanying benefit of this strategy is the parallel increase in pH, thus counteracting ocean acidification (Ilyina et al., 2013;  
61 Köhler et al., 2010).

62 Tests for OAE under close-to-natural conditions are still scarce (Albright et al., 2016; Cyronak et al., 2023; Ferderer et al.,  
63 2022; Paul et al., 2023; Sánchez et al., 2023; Yang et al., 2023). For a safe and efficient application of OAE, it is crucial to  
64 assess the induced changes in carbonate chemistry and investigate their potential environmental impacts (Bach et al., 2019;  
65 Riebesell et al., 2023).

66 In isolated case studies, prototypes for alkalinity enhancement have already been put into practice to counteract lake  
67 acidification (e.g., Koch & Mazur, 2016; LMBV, 2017) or were discussed in context of river water alkalinity enhancement  
68 (Sterling et al., 2023). Various application methods for OAE ranging from spreading grinded rock powder or mineral phases  
69 (Kheshgi, 1995) to liquid addition of alkaline solutions directly into the seawater or via rivers (Hartmann et al., 2013; Sterling  
70 et al., 2023), and electrochemical alkalinity generation (Eisaman et al., 2023; Renforth & Henderson, 2017) have been  
71 proposed. Alkalinity enhancement could be achieved in a CO<sub>2</sub>-equilibrated or non-CO<sub>2</sub>-equilibrated manner, as discussed in  
72 Schulz et al. (2023). In the non-equilibrated scenario, the seawater would gradually equilibrate over time by absorbing  
73 atmospheric CO<sub>2</sub>. The CO<sub>2</sub>-equilibrated approach consists of adding alkalized water that is already in equilibrium with the  
74 atmosphere. This means that at the point of addition, the water is put into equilibrium with the atmosphere either with  
75 technological apparatus before release or a CO<sub>2</sub> source is used to bring the water into equilibrium after TA addition.  
76 Alternatively, solids like Na<sub>2</sub>CO<sub>3</sub> or NaHCO<sub>3</sub> could be used for OAE since they are already used to capture CO<sub>2</sub> from a source  
77 (e.g., Forster 2012, 2014) before the alkaline products are disposed of.



78 To illustrate the impact of different alkalinity addition scenarios on various carbonate chemistry parameters, Figure 1 presents  
 79 a TA:DIC diagram modelled after Deffeyes (1965). Besides dissolved inorganic Carbon (DIC) and total alkalinity, the  
 80 Deffeyes diagram provides information on corresponding pH,  $p\text{CO}_2$ , and saturation state for aragonite ( $\Omega_{\text{aragonite}}$ ).  
 81 Surpassing critical thresholds of  $\Omega_{\text{aragonite}}$  saturation states for a certain period of time could result in  $\text{CaCO}_3$  precipitation  
 82 (Schulz et al., 2023; Zeebe & Wolf-Gladrow, 2001). This phenomenon could lead to a runaway process, as observed in  
 83 laboratory-based experimental studies conducted by Moras et al. (2022), Hartmann et al.

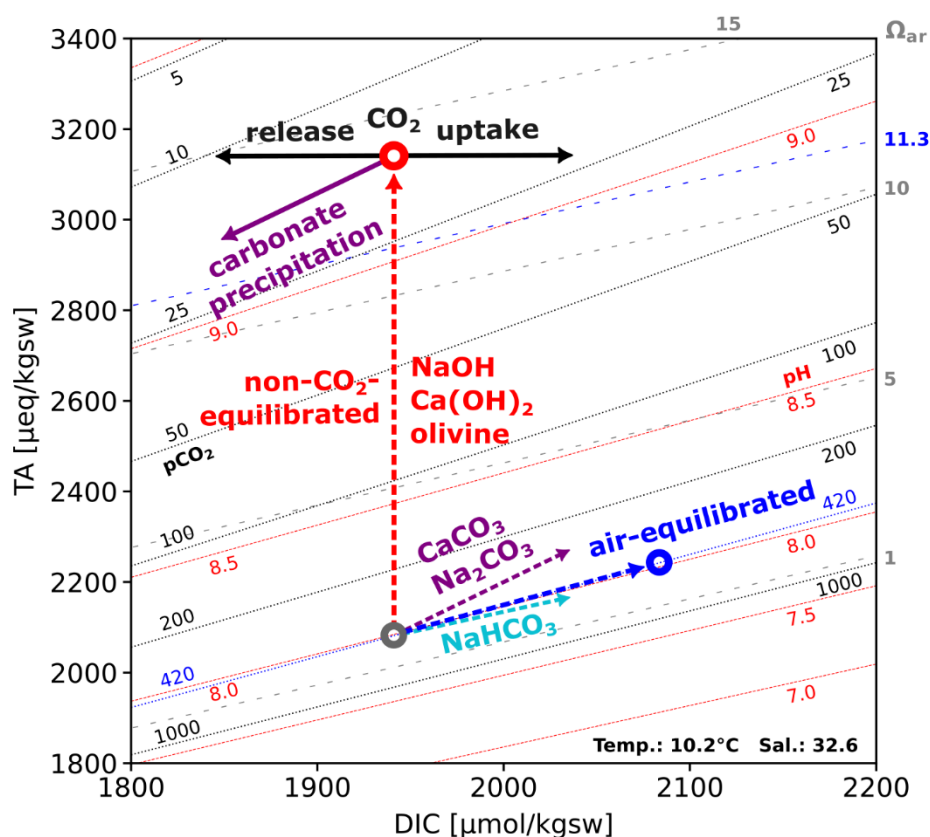


Figure 1: Example of a TA:DIC diagram after Deffeyes, 1965, in context of OAE; background contours represent iso-lines of pH (red),  $\Omega_{\text{aragonite}}$  (dotted grey) and  $p\text{CO}_2$  (black) values; shown contours reflect pH,  $p\text{CO}_2$  and  $\Omega_{\text{aragonite}}$  values for varying TA and DIC levels at given temperature and salinity conditions; dashed arrows show the impact of indicated alkalization approaches, e.g. non- $\text{CO}_2$ -equilibrated TA addition could be realized by injection or dissolution of sodium hydroxide (NaOH), an air-equilibrated TA addition (in an equilibrium to the atmosphere –  $p\text{CO}_2$  420ppm) could be achieved by utilizing a combination of  $\text{NaHCO}_3$  and  $\text{Na}_2\text{CO}_3$ ; during non- $\text{CO}_2$ -equilibrated approaches the  $p\text{CO}_2$  of the manipulated water is reduced, creating the potential of  $\text{CO}_2$  uptake (black arrow) from the atmosphere; if the TA addition surpasses



certain critical ranges (for surface free waters under the given conditions here indicated by the blue  $\Omega_{\text{aragonite}}$  contour of 11.3, calculated after Marion et al. (2009)), carbonate precipitation (purple arrow) results in the reverse changes of  $\text{CaCO}_3$  dissolution

84 (2023), Fuhr et al. (2022), and Pan et al. (2021). This process could lead to a net loss in  $\text{CO}_2$ -storage potential and will result  
85 in a leakage of TA and DIC.  
86 Considering the complexity and variety of possible environmental impacts of OAE scenarios, systematic empirical  
87 investigations of alkalization approaches seem to be vital providing meaningful sustainability assessments. This study aims  
88 to assess the geochemical impacts of alkalinity addition in seawater by refining and improving upon the experimental setup of  
89 Hartmann et al. (2023), testing  $\text{CO}_2$ -equilibrated and non-equilibrated TA enhancement scenarios in natural seawater.  
90 Incubation experiments were conducted with extended TA ranges and runtimes, along with increased sampling frequency and  
91 enhanced resolution of the TA gradients. Experiments were designed to identify stability ranges of the added alkalinity and  
92 characterize critical thresholds that trigger the runaway precipitation process.



## 93 2 Methods

### 94 2.1 Experimental setup

95 Four sets of experiments were conducted between May and July 2022 using natural seawater from the Raunefjord (60.27°N,  
96 5.20°E) close to the Espeland Marine Biological Station (Bergen, Norway). All four experiments used the same setup. 250 ml  
97 polystyrene cell culture bottles were filled with filtered seawater in a flow-through incubation box (PMMA) and incubated  
98 outdoors to follow the local light conditions. The box was covered in blue foil (172 Lagoon Blue foil, Lee filters, Burbank,  
99 CA, United States) to mimic the light conditions in the fjord at a depth of ~5 m. The temperature was regulated by recirculating  
100 fjord water in the incubation box, thus ensuring that the incubation temperature matched that of the fjord. To prevent the  
101 occurrence of substantial headspace throughout the experiment, each treatment level was divided into 3-4 separate bottles. The  
102 division allowed for progressive volume removal during sampling while reducing the potential for gas exchange processes.  
103 Within each experiment, a new set of bottles was opened sequentially after 3-4 samplings. Alkalinity was enhanced using a  
104 0.5 M NaOH (sodium hydroxide) stock solution for the non-CO<sub>2</sub>-equilibrated and a combination of NaHCO<sub>3</sub> (sodium  
105 bicarbonate, 0.4 M) and Na<sub>2</sub>CO<sub>3</sub> (sodium carbonate, 0.2 M) stock solutions for the preparation of the CO<sub>2</sub>-equilibrated  
106 treatments. The latter were adjusted to attain equilibrium with the surrounding air's CO<sub>2</sub> concentration (~420 ppm). For each  
107 of the two, the experimental setups encompassed: 1. abiotic conditions, achieved by removing organisms via filtration through  
108 a 0.2 µm filter, 2. biotic where only the small phytoplankton community was included by using a 50 µm filter mesh to remove  
109 larger particles and organisms. An overview of the reached TA-levels and step sizes, runtimes and temperature ranges is given  
110 in Table 1. The experiments were conducted over a span of two months, with each incubation run for 20 or 25 days. The  
111 experiments were therefore partially temporally separated, resulting in slight variations in starting conditions and average  
112 temperatures, ranging from 10 to 16°C. Biotic and abiotic treatments were simultaneously conducted within each equilibration  
113 mode. The initial carbonate chemistry parameters of the collected seawater before manipulation were relatively constant for  
114 all approaches (TA<sub>initial</sub> ~2190 ± 5 µeq kgsw<sup>-1</sup>, DIC ~1890 ± 5 µmol kgsw<sup>-1</sup>, pH ~8.2 ± 0.02, Sal. ~32.6 ± 0.1).



115

Table 1: Overview experimental design Bergen 2022

#	Seawater conditions	CO <sub>2</sub> state to atmosphere	Alkaline material	Runtime [days]	Range TA <sub>added</sub> [μeq kgsw <sup>-1</sup> ]	TA <sub>added</sub> gradient steps [μeq kgsw <sup>-1</sup> ]	Temperature [°C]
I	biotic	air-equilibrated	Na <sub>2</sub> CO <sub>3</sub> / NaHCO <sub>3</sub>	20	0-2800	200	12-15
	abiotic			20	0-9200	200/800	12-16
II	biotic	non-equilibrated	NaOH	25	0-2800	200	10-11
	abiotic			25	0-3400	200	11-13

116

## 2.2 Sampling and measurements

117

For carbonate chemistry analysis, 40-50 ml of incubated water were taken per sampling day and treatment level. Using a peristaltic pump connected to a 0.2 μm syringe filter, samples were filtered immediately to stop further reactions, remove particles and prepare each sample for measurements. All treatments were measured without replicates for TA, pH, temperature and salinity, and biotic treatments were further analysed to assess the biological responses. An accompanying publication is going to describe the impact of enhanced alkalinity on the included phytoplanktonic communities during the first 6 days of the biotic incubation experiments. A selection of filtrates was saved for scanning electron microscopy (SEM) analysis. Minor shifts in pH, DIC and  $\Omega_{\text{aragonite}}$  originate from increasing water temperatures during the runtimes of the experiments, photosynthetic activity in the biotic approaches or minor ingassing from the headspace of the reactor bottles.

125

Methods and devices for measuring TA, pH, temperature, and salinity were identical to experiments I and II from Hartmann et al. (2023). Total alkalinity was determined by titration with a 0.02M hydrochloric acid, using an 888 Titrande autosampler (Metrohm). TA measurements were corrected against certified reference materials (CRM batch 193), supplied by Prof. Andrew G. Dickson laboratory, Scripps Institution of Oceanography (USA). A WTW multimeter (MultiLine® Multi 3630 IDS) was used to measure pH (SenTix 940 pH-electrode), temperature and salinity (TetraCon 925 cell, Xylem). The pH-probe was calibrated with WTW buffer solutions according to NIST/PTB in four steps (1.679–9.180 at 25 °C) and corrected for seawater after Badocco et al. (2021). DIC, pCO<sub>2</sub> and saturation states were calculated using CO2SYS Excel version 2.5 (Pierrot et al., 2006), including error propagations based on Orr et al. (2018). Constants in CO2SYS were set to Lueker et al. (2000) for K<sub>1</sub> and K<sub>2</sub>, Dickson (1990) for KHSO<sub>4</sub>, and Perez and Fraga (1987) for KHF and Lee et al. (2010) for [B]<sub>T</sub> Value, and the pH was calculated on the total scale.

134



135 The physical appearance of precipitated particles and their elemental composition were analyzed by two separate SEM setups:  
136 1. Tabletop Microscope Hitachi TM4000plus (University of Hamburg) and 2. Zeiss Gemini Ultra55 Plus at (CAU Kiel), both  
137 equipped with an energy-dispersive X-ray spectroscopy (EDX) detector.  
138

### 139 **2.3 $\Delta$ TA equation**

140 Based on the concept from Hartmann et al. (2023), the subsequent equation is utilized to simplify the characterization of  
141 reached values or alterations in TA:  
142

$$143 \quad \Delta TA_{net} = TA_{final} - TA_{initial} = \Delta TA_{added} + \Delta TA_{loss}$$

144  $\Delta TA_{net}$ : net change of TA

145  $TA_{final}$ : absolute reached TA after TA addition (measured)

146  $TA_{initial}$ : initial TA of used seawater (measured)

147  $\Delta TA_{added}$ : amount of increased TA by alkalinity addition

148  $\Delta TA_{loss}$ : amount of TA decline during the experiment (negative sign)





149 **3 Results**

150 **3.1 CO<sub>2</sub> equilibrated experiments**

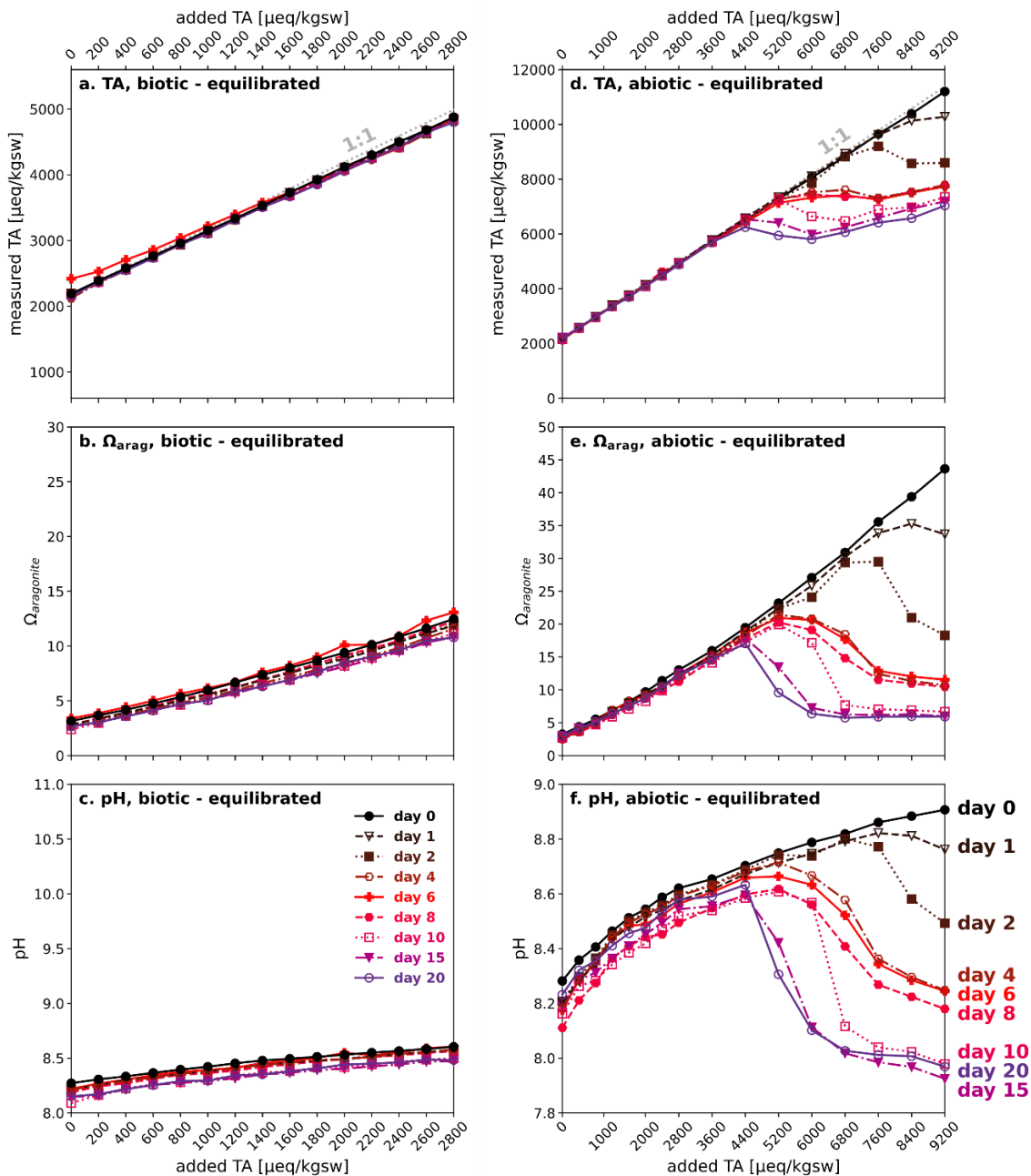




Figure 2: Temporal TA,  $\Omega_{\text{aragonite}}$  and pH evolution in CO<sub>2</sub>-equilibrated experiments, under biotic (left) and abiotic (right) conditions; each diagram represents a specific carbonate chemistry parameter investigated, i.e., measured TA (a. and d.),  $\Omega_{\text{aragonite}}$  (b. and e.) and pH (c. and f.) as a function of added TA and time point; legends for sampling days are given in c. (biotic) and f. (abiotic); initial conditions of the used seawater before manipulation: TA<sub>initial</sub> ~2190  $\mu\text{eq kgsw}^{-1}$ ,  $\Omega_{\text{aragonite}}$  ~2.5-3.0, pH ~8.2, Sal. ~32.6, biotic: Temp. 12-15°C, abiotic: 12-16°C; be aware of the differing scales on the y-axes for each show parameter

151

152 In the biotic CO<sub>2</sub>-equilibrated experiment an air-equilibrated alkalization of up to 2800  $\mu\text{eq kgsw}^{-1}$  could be achieved during  
153 the 20-day runtime. All carbonate chemistry parameters remained constant, showing that a TA addition slightly above the  
154 estimated critical  $\Omega_{\text{aragonite}}$  value for pseudo homogenous precipitation of 11.3 (after Marion et al., 2009) could be achieved.  
155 This level was maintained for 20 days without causing any CaCO<sub>3</sub> precipitation, as illustrated in Fig. 2a-c.

156 By extending the alkalinity range up to 9200  $\mu\text{eq kgsw}^{-1}$  in the abiotic air-equilibrated experiment  $\Omega_{\text{aragonite}}$  values far above  
157 critical levels were reached, resulting in extensive carbonate precipitation in a runaway style (Fig. 2d-f). All targeted alkalinity  
158 levels were achieved ~3min after alkalinity addition (day 0), and a decline in TA was observed in treatments above  $\Delta\text{TA}$  3600  
159 (corresponding to  $\Omega_{\text{aragonite}}$  of 14.6). Starting with the highest treatment levels after 1 day, precipitation was triggered in all  
160 batches with a  $\Delta\text{TA}$  above 3600 over the runtime of 20 days (see Fig. 2d). Following precipitation, once  $\Omega_{\text{aragonite}}$  reached  
161 values of 5.8-6.0, the process halted, resulting in a linear alignment of final TA values. The TA loss rate was significantly  
162 reduced towards the end of the precipitation procedure; however, it could not be excluded that the process would have  
163 continued if the experiment had proceeded. Despite substantial total alkalinity loss attributed to runaway precipitation, all  
164 treatments involving secondary mineral formation still achieved a net gain in TA ranging from 3600 to 4850  $\mu\text{eq kgsw}^{-1}$ .  
165 Nevertheless, pH values in batches which underwent the precipitation process were accompanied by an acidification below  
166 the initial seawater pH level.



167 3.2 Non-CO<sub>2</sub>-equilibrated experiments

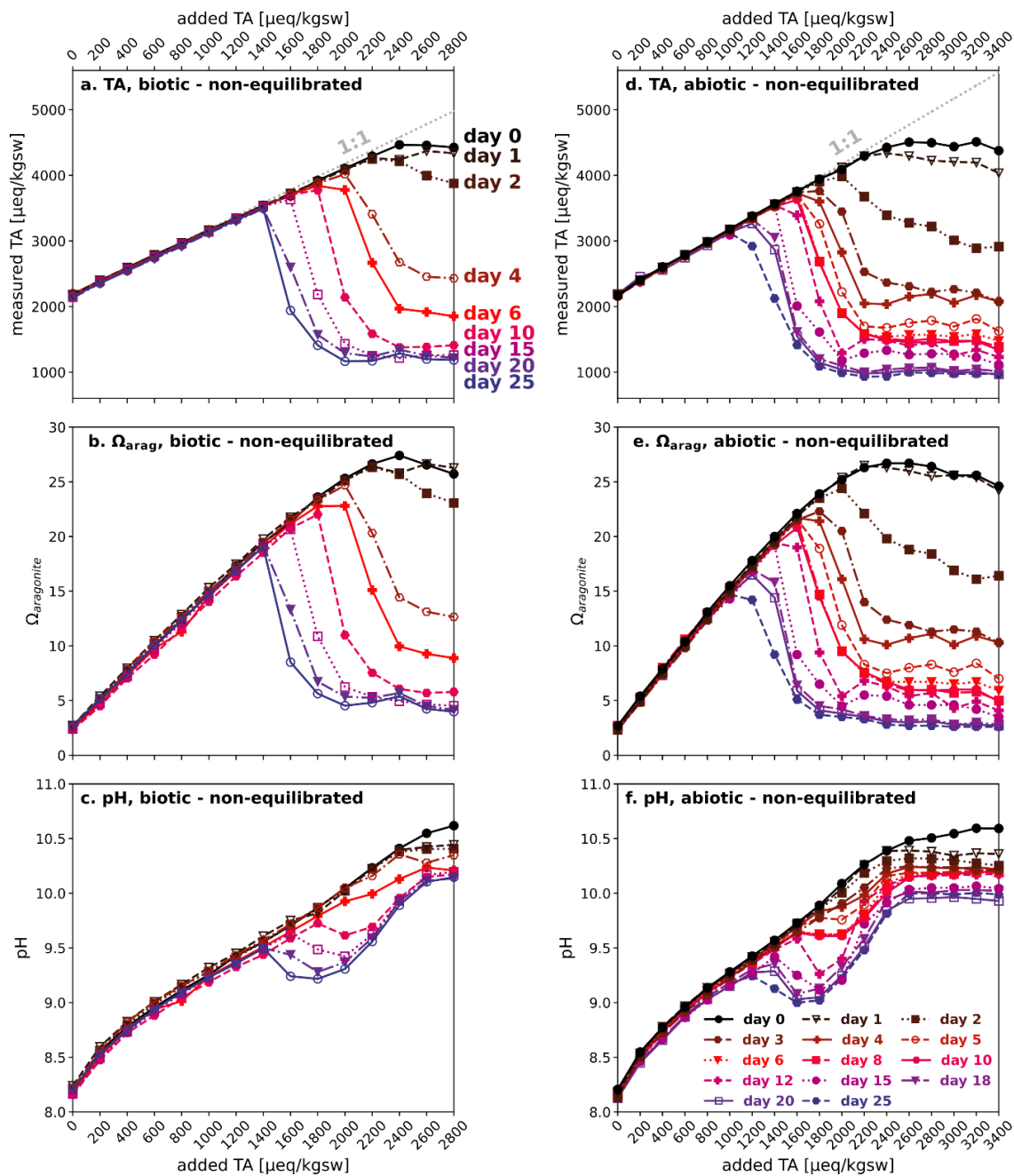




Figure 3: Temporal TA,  $\Omega_{\text{aragonite}}$  and pH evolution of non-CO<sub>2</sub>-equilibrated experiments, biotic (left) and abiotic (right); each graph represents a specific sampling day; initial conditions of the used seawater before manipulation: TA<sub>initial</sub> ~2190  $\mu\text{eq kgsw}^{-1}$ ,  $\Omega_{\text{aragonite}}$  ~2.5-3.0, pH ~8.2, Sal. ~32.6, biotic: Temp. ~10-11°C, abiotic: Temp. ~11-13°C

168

169 Alkalinity enhancement in the biotic and abiotic non-CO<sub>2</sub>-equilibrated experiments achieved a steady increase up to an addition  
170 of 2400  $\mu\text{eq kgsw}^{-1}$  at day 0 (Fig. 3). Under the given local conditions (Temp. 10-11°C, Sal. 32.6), exceeding the TA<sub>target</sub> level  
171 of 4570  $\mu\text{eq kgsw}^{-1}$  led to a drop back to 4450 ± 60  $\mu\text{eq kgsw}^{-1}$  after ~3min, irrespective of the quantity of further added  
172 alkalinity. For the biotic non-CO<sub>2</sub>-equilibrated approach (Fig. 3a-c) treatments from  $\Delta\text{TA}$  1400 to 2800 showed a decrease in  
173 alkalinity during the subsequent 25-day runtime, as a consequence of secondary mineral formation. The precipitation process  
174 uniformly came to halt in a range of 1230 ± 60  $\mu\text{eq kgsw}^{-1}$ , corresponding to an  $\Omega_{\text{aragonite}}$  of 4-5. A similar behavior was  
175 observed in the abiotic non-CO<sub>2</sub>-equilibrated experiment (Fig. 3d-f). Slightly higher water temperatures (11-13°C) in  
176 comparison to the biotic approach (10-11°C), potentially led to an earlier decline of alkalinity and lower final in TA (1030 ±  
177 60  $\mu\text{eq kgsw}^{-1}$ ) and  $\Omega_{\text{aragonite}}$  (2.5-4). All treatment levels from  $\Delta\text{TA}$  1200 to 3400 showed precipitation during the 25-day  
178 runtime. Unlike the abiotic CO<sub>2</sub>-equilibrated approach, the runaway precipitation in both non-equilibrated experiments resulted  
179 in a net-loss of alkalinity, while pH values remained in a range of 9.0-10.1. Nevertheless, despite relatively high  $\Omega_{\text{aragonite}}$  values  
180 of up to ~17 (biotic) and ~15 (abiotic) in the non-CO<sub>2</sub>-equilibrated experiments, after 25 days the alkalinity was still constant  
181 in all treatments below  $\Delta\text{TA}$  1200.

### 182 3.3 TA:DIC diagrams

183 TA:DIC diagrams in Fig. 4a-e provide a contextualized overview of trend and temporal development of carbonate chemistry  
184 parameters. Simultaneous TA and DIC enhancement in the CO<sub>2</sub>-equilibrated experiments led to the characteristic diagonal  
185 gradient, while non-CO<sub>2</sub>-equilibrated approaches resulted in a straight vertical increase in TA as a consequence of OH<sup>-</sup>  
186 injection (also see Fig. 1). Treatments exhibiting secondary carbonate formation followed the strict 2:1- $\Delta\text{TA}:\Delta\text{DIC}$  decline  
187 ratio during the precipitation phase, leading to a consistent alignment of data points in straight trend trajectories. The tendency  
188 for consistent linear trends in TA/DIC during alkalization and precipitation processes in the conducted experiments, allows  
189 to visually trace the origin of shapes and temporal development trends of pH and  $\Omega_{\text{aragonite}}$  in Figures 2 and 3 by utilizing  
190 exhibited TA:DIC diagrams. For example, the consistency of  $\Omega_{\text{aragonite}}$  values within treatments that underwent the runaway  
191 process allows to predict the final state of other carbonate chemistry parameters, oriented on the shape and position of the  
192 related  $\Omega_{\text{aragonite}}$  contour (see Fig. 4b-e). The immediate drop back to 4450 ± 60  $\mu\text{eq kgsw}^{-1}$  in both non-CO<sub>2</sub>-equilibrated  
193 experiments showed a consistent pattern in dislocation of target and measured TA and DIC values, following a steady declining  
194  $\Delta\text{TA}:\Delta\text{DIC}$  loss ratio of 4.9-2.3 from highest to lowest target alkalinity levels (Fig. 4f), indicating the formation of non-  
195 carbonate-bearing secondary phases, as Mg(OH)<sub>2</sub> (also see section 4.3).

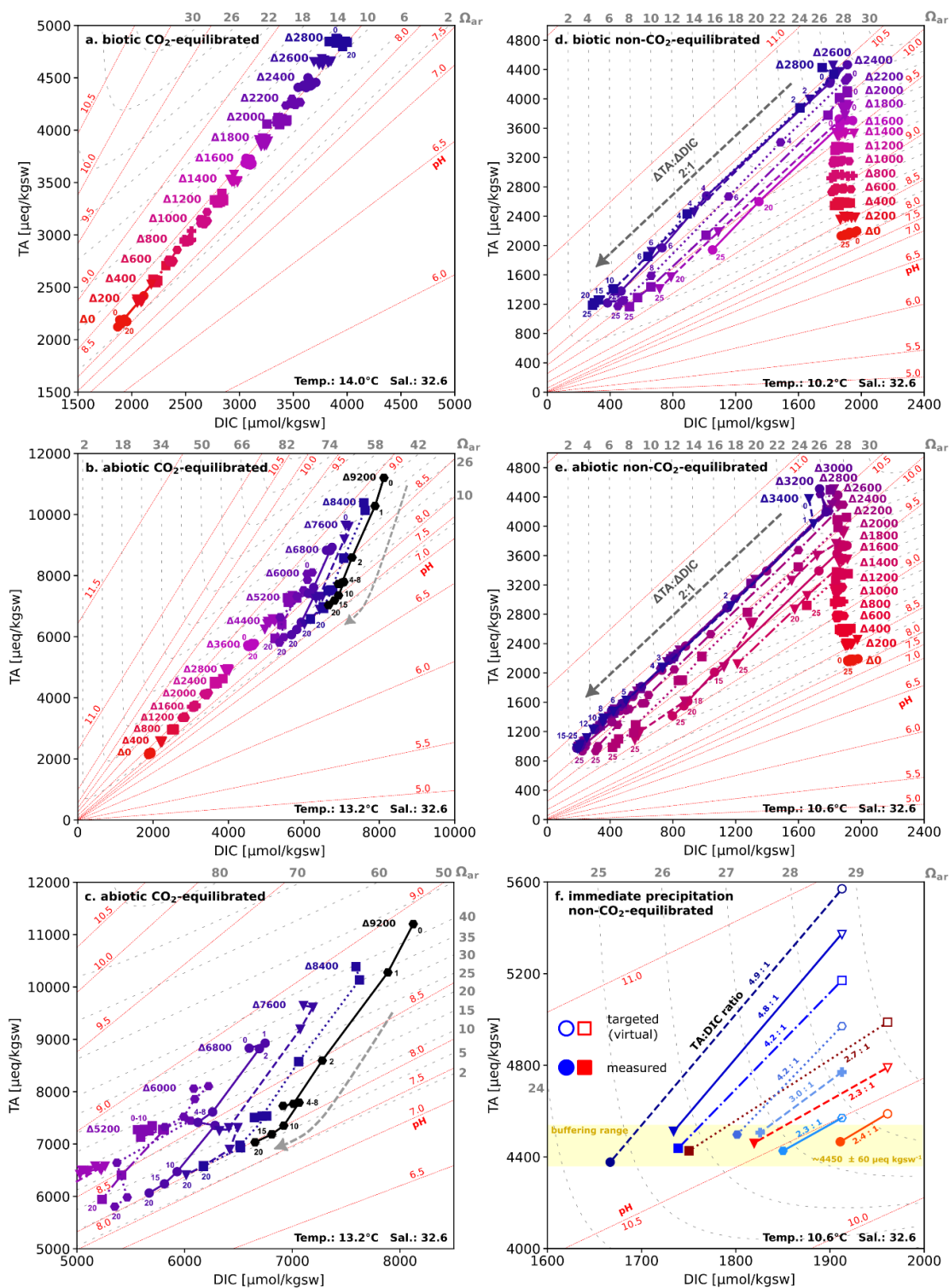




Figure 4: TA:DIC diagrams (a.) CO<sub>2</sub>-equilibrated (biotic), (b.) CO<sub>2</sub>-equilibrated (abiotic), (c.) zoom into precipitating treatments in (b.), (d.) non-CO<sub>2</sub>-equilibrated (biotic), (e.) non-CO<sub>2</sub>-equilibrated (abiotic), a selection of data points is labeled with their corresponding sampling day; (f.) comparison of targeted and measured values for treatments with immediate precipitation (blue) abiotic (red) biotic non-CO<sub>2</sub>-equilibrated, indicating the formation of a non-carbonate phase like Mg(OH)<sub>2</sub>; note that due to varying temperatures during the experiments, given the  $\Omega_{\text{aragonite}}$  and pH contours in all diagrams are temperature and salinity-dependent, potentially resulting in slight inaccuracies in showing exact values for individual data points

### 196 3.4 TA loss rates

197 TA-loss rates for treatments which underwent the precipitation process exhibited similar relationships, independent of the  
198 CO<sub>2</sub>-equilibration state. In regular patterns, elevated initial TA-levels induced an earlier initiation of the exponential decay  
199 process accompanied by increased TA loss rates within each experiment (see Figs. 5 and S4). Absolute rates were dependent  
200 on the potential for TA loss within each treatment, regulated by the initial DIC and  $\Omega_{\text{aragonite}}$  values. Irrespective of the initial  
201 TA-level, treatments that showed an immediate precipitation in both non-CO<sub>2</sub>-equilibrated experiments exhibited almost  
202 identical development trends during the precipitation process. Figure 6 showcases the related temporal TA development of the  
203 abiotic CO<sub>2</sub>-equilibrated and biotic non-CO<sub>2</sub>-equilibrated approaches. Outlier values from the few sampling days were  
204 excluded for the calculation of TA loss rates in the abiotic CO<sub>2</sub>-equilibrated and abiotic non-CO<sub>2</sub>-equilibrated experiments.  
205 For details see section “outliers” in the supplements.

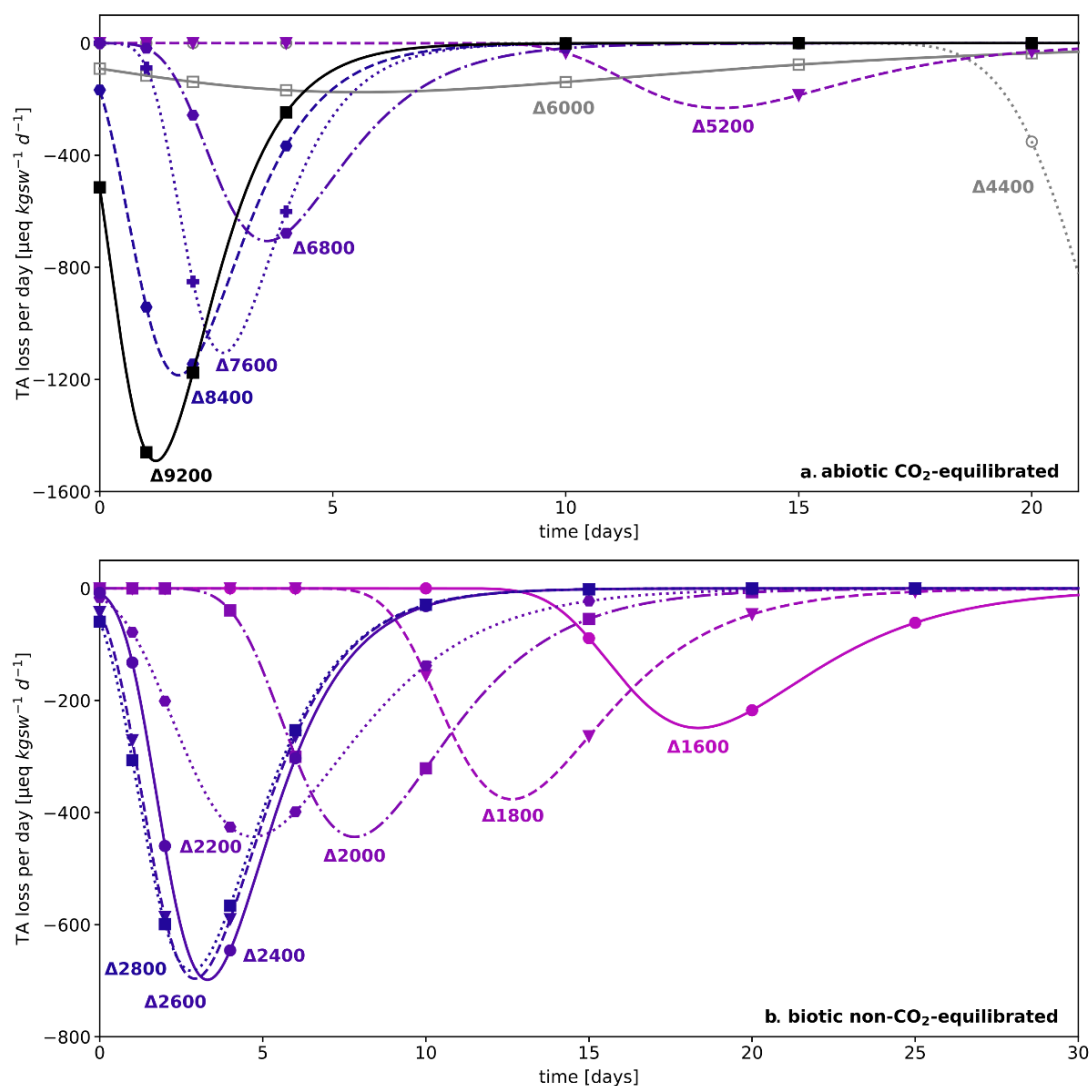


Figure 5: TA loss rates per day in (a.) abiotic  $\text{CO}_2$ -equilibrated and (b.) biotic non- $\text{CO}_2$ -equilibrated experiments showing precipitation processes, rates were calculated based on differentiating functions determined by a sigmoidal curve fit model of the temporal development of TA (see Fig. 6); due to missing data points, rates for treatment levels  $\Delta 4400$  and  $\Delta 6000$  in (a.) could not be determined. Regarding  $\Delta \text{TA} 6000$  see description of outliers in the supplements; for TA loss rates of the abiotic non- $\text{CO}_2$ -equilibrated experiment see Fig. S4

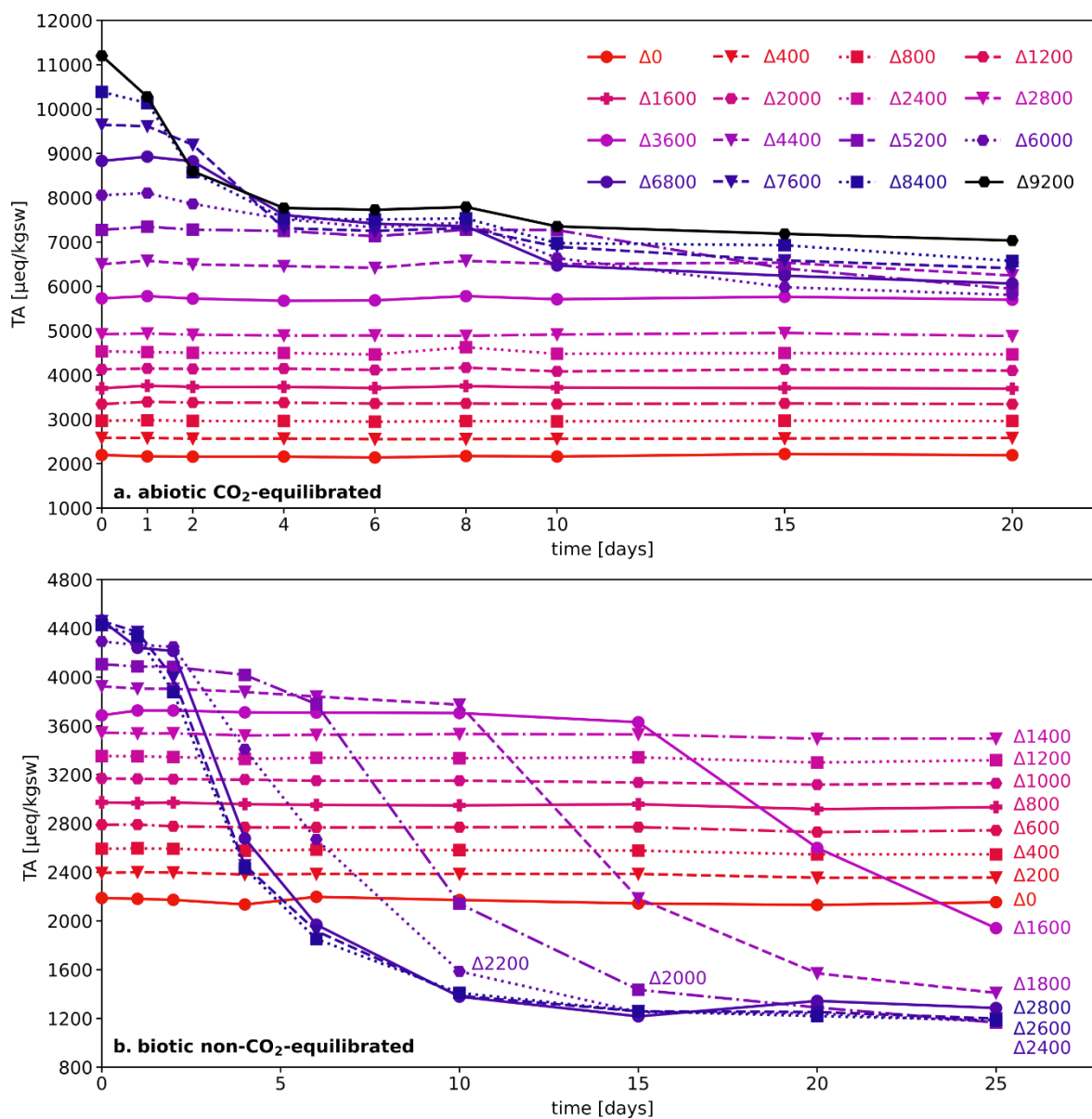


Figure 6: Temporal development of TA in (a.) abiotic  $\text{CO}_2$ -equilibrated approaches and (b.) biotic non- $\text{CO}_2$ -equilibrated experiments; compare to related TA loss rates in Fig. 5; see Fig. S2 and S3 for the biotic  $\text{CO}_2$ -equilibrated and the abiotic non- $\text{CO}_2$ -equilibrated approaches





### 207 3.5 SEM

208 SEM images of the filtered residua of the experiments show a variety of common shapes of aragonite precipitates. Throughout  
209 all conducted experiments in this study visual identifiable precipitates only appeared in treatments which also exhibited a  
210 decline in TA. The morphologies of the particles in the CO<sub>2</sub>-equilibrated and non-CO<sub>2</sub>-equilibrated treatments were identical  
211 if secondary mineral formation was triggered. The quantity, structures and shapes of the particles evolved with increased  
212 alkalinity. Figure 7 provides examples of different development stages over the runtime of 6 days in the non-CO<sub>2</sub>-equilibrated  
213 biotic experiment. The bulk of particles showed central stems, which branched out to each end. Morse et al. (2007) described  
214 the more developed shapes as “broccoli” structures, due to its physical appearance, while Nielsen et al. (2014) entitled the less  
215 branched shapes as “sheaf-of-wheat” bundle. These symmetric particles were the dominant appearing shapes of secondary  
216 phases. Treatment levels with initial precipitation showed early stages of stem-like structures with no or very little branching.  
217 With higher alkalinity addition more advanced shapes and sizes were predominant, characterized by progressive outbranching.  
218 Most developed stages exhibited a merging of the fanned out ends to form closed spheres. Next to the dominant simple stems,  
219 multipolar particles, with up to six branches were observed, at all development stages. Despite the variable initial branching  
220 numbers, the growth behavior followed the same patterns. Following the scheme presented in Fig. 7 all variants finally reached  
221 a closed structure. Observed ellipsoid shaped particles might indicate that the previous precipitate was bi-polar, while more  
222 spherical ones had a multi-polar origin. No indications for hollow stems, like described in Hartmann et al. (2023), could be  
223 observed. Sizes vary from 2-5 μm for initial shapes, to 10-30 μm for non-closed “broccoli” particles and up to 80 μm for  
224 complete spherical forms. For an overview of occurrence and distribution of particle sizes and shapes see Fig. 8(a-f).  
225 Consistently higher loss of TA during the runaway process resulted in greater numbers and more developed stages in the  
226 precipitates. EDX-analysis uniformly identified the precipitates as Ca-dominated carbonates (Ca: 7.8-12.3 mol%, Mg: 2.1-5.3  
227 mol%, C: 13.7-25.8 mol%, O: 61.0-66.2 mol% - Zeiss Gemini Ultra55 Plus (CAU)) with indications of a relatively high  
228 content of Mg carbonates phases.

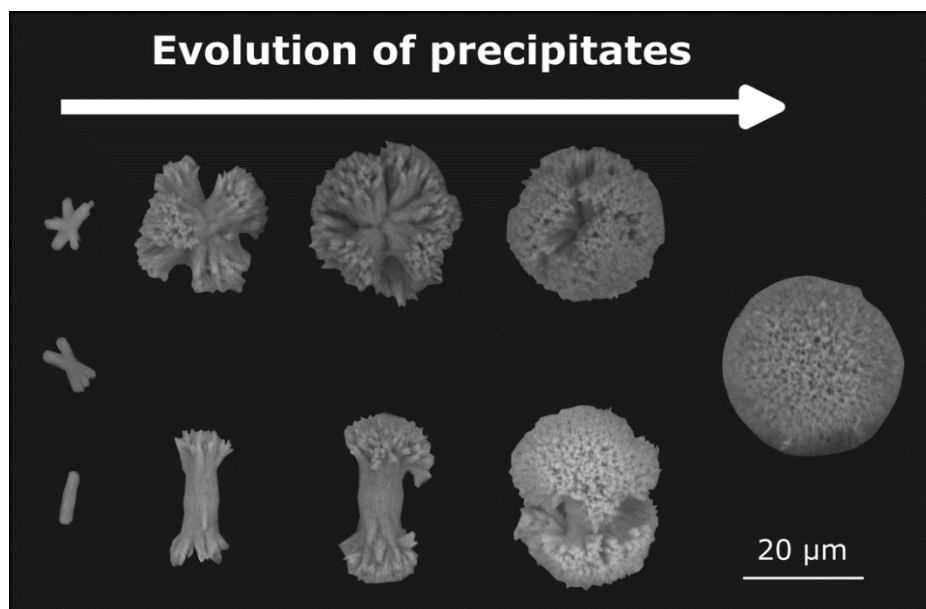


Figure 7: Scheme of the evolution of precipitates, showing a selection of precipitated particles in different development stages. Growth of the initial “stem” structure is accompanied by outbranching on each end. Independent of the polarity of the initial stems, developed particles uniformly form spherical shapes, Tabletop Microscope Hitachi TM4000plus (UHH)

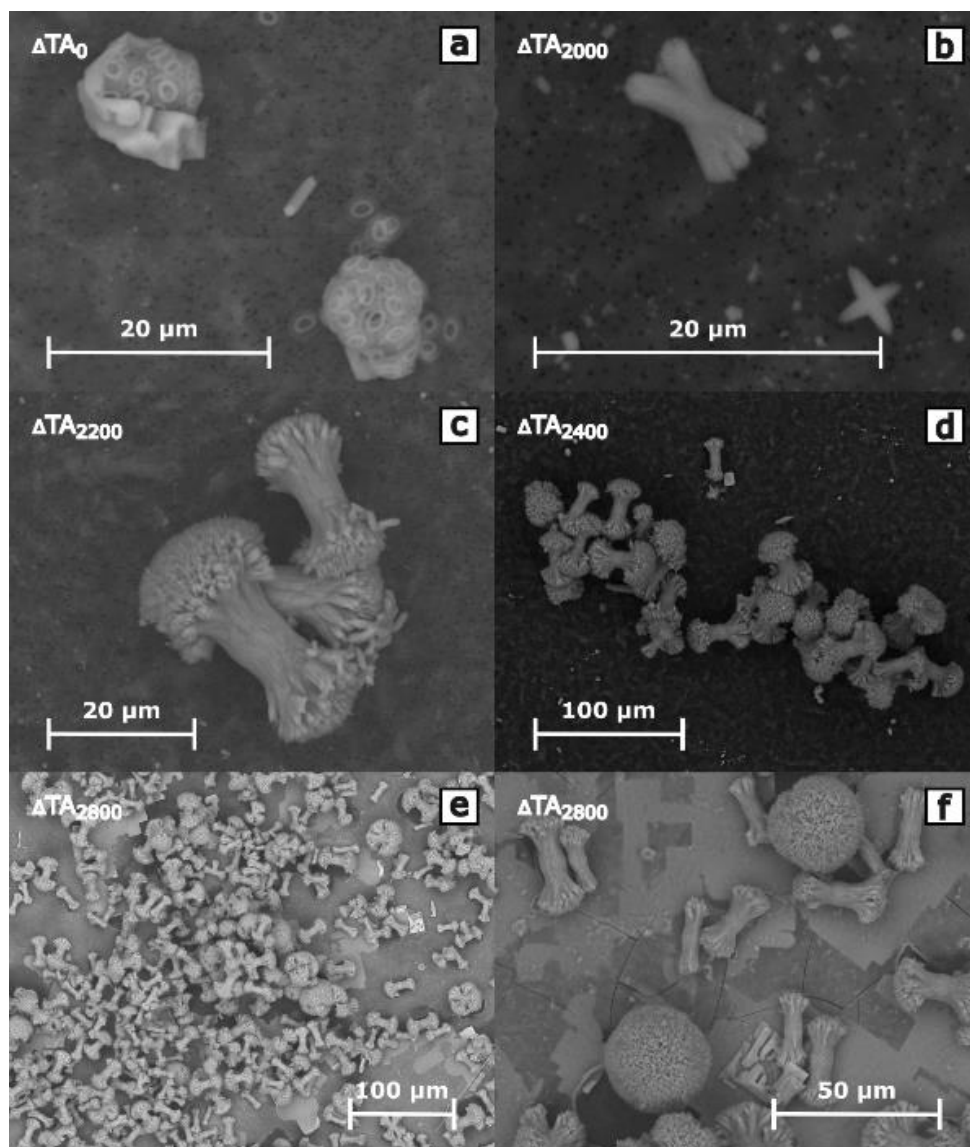


Figure 8: SEM images, overview of shapes and occurrences of precipitates in the biotic non-CO<sub>2</sub>-equilibrated treatments; no difference could be determined in shapes and appearance within other experiments; compare to Boon et al. (2020), Morse et al. (1997), Pan et al. (2022), Nielsen et al. (2014) and Hartmann et al. (2023), who showed similar shaped carbonate/aragonite precipitates, Tabletop Microscope Hitachi TM4000plus (UHH)



## 231 4 Discussion

232

233 The stability of achieved TA enhancements varied from several hours to weeks, depending primarily on the resulting  $\Omega_{\text{aragonite}}$ ,  
234 the CO<sub>2</sub>-equilibration state, local environmental conditions, and the quantity of introduced alkalinity. While target TA levels  
235 were achieved within acceptable tolerances, treatment levels exceeding pH values of approximately 10.3 failed to achieve the  
236 intended TA values when measured within three minutes after application. Such observation is potentially the result of  
237 immediate magnesium hydroxide formation, buffering the injected alkalinity, as indicated by Eisaman et al. (2023) and  
238 Cyronak et al. (2023). While runaway calcium carbonate formation was demonstrated in previous research (Moras et al., 2022;  
239 Hartmann et al., 2023), a systematic description of TA loss with respect to time and saturation state could be established here.  
240 This allows for the prediction of TA loss behavior when local environmental parameters are well-defined. Consequently, such  
241 systematic studies will provide needed parameterized functions for models to assess the consequences of OAE before  
242 application (Fennel et al., 2023). Together with addressing the mixing of treated and untreated water, ultimately diluting the  
243 additional seawater TA, an assessment of the stability of alkalinity could be generated, if sufficient systematic studies were  
244 conducted. Remarkably in the CO<sub>2</sub>-equilibrated approach for additions of up to 3600  $\mu\text{mol kgsw}^{-1}$ , no TA loss was observed  
245 within the first 20 days, highlighting the relevance of the equilibration state of the carbonate system for the stability of  
246 alkalinity.

247

### 248 4.1 Runaway CaCO<sub>3</sub> precipitation

249 While the objective of this study was to detect stable alkalinity ranges, exceeding critical limits caused runaway carbonate  
250 formation, which leveled out at a new equilibrium. EDX-analysis of the precipitates (see section 3.5) and the 2:1  $\Delta\text{TA}:\Delta\text{DIC}$   
251 decline ratios (Fig. 4) confirmed the formation of CaCO<sub>3</sub> phases when pH-values were below 10.3.

252 Independent of the CO<sub>2</sub>-equilibration state or initial treatment level, the temporal TA development patterns after the start of  
253 runaway precipitation could be fitted with a sigmoidal function. Start of runaway precipitation, TA loss rate, and duration of  
254 TA decline (Figs. 2-6) varied with temperature and initial TA and DIC treatment levels, but followed a general pattern (see  
255 Fig. 9):

- 256 1. nucleation phase – stage of generation or provision of sufficient surface area to trigger the runaway process
- 257 2. precipitation phase – stage of exponential decay in TA and DIC in a 2:1 ratio, due to the runaway process, until the  
258 potential declines significantly with reduced  $\Omega_{\text{aragonite}}$  values
- 259 3. new equilibrium - final state after the runaway process ended where the changes in TA and DIC might be too low  
260 to be measured

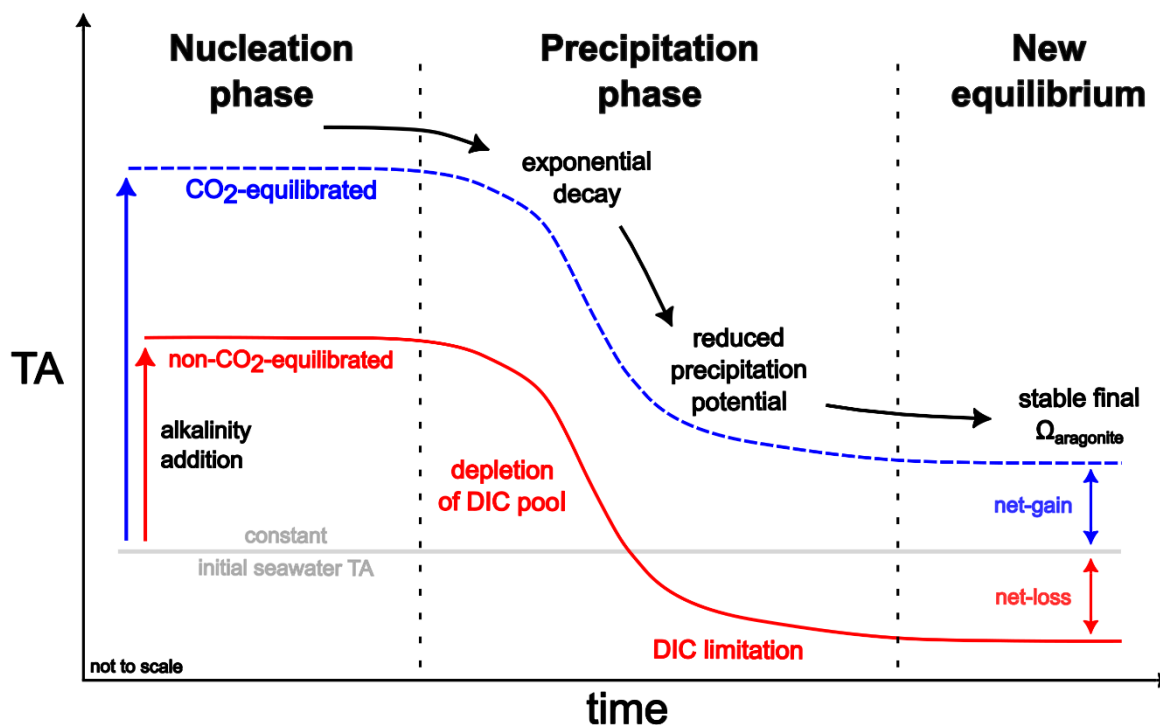


Figure 9: Concept of carbonate runaway precipitation, showing the generalized evolution of TA for non-CO<sub>2</sub>-equilibrated and CO<sub>2</sub>-equilibrated alkalinity addition scenarios, deduced from experimental results of this study (not to scale). As nucleation is a time dependent process, despite overcritical  $\Omega_{\text{aragonite}}$  values, a stable temporal state without observable precipitation exists, depending on the physicochemical conditions ranging from seconds to years. While the secondary carbonate formation in the non-CO<sub>2</sub>-equilibrated treatments result in TA values below the initial seawater levels, CO<sub>2</sub>-equilibrated treatments might, despite a substantial TA loss during the runaway process, achieve a net gain in alkalinity. For further descriptions see text.

261

#### 262 4.1.1 Nucleation phase

263 The duration of the nucleation phase varies depending on the quantity and form of added alkalinity, and the alterations in the  
264 saturation state, in this work ranging from immediate precipitation to several weeks. However, the nucleation phase might last  
265 as long as thousands of years (c.f., Pytkowicz, 1973). To date, only a small amount of data is available to parameterize the  
266 duration of this phase systematically. These data are needed for models to assess the consequences of OAE applications (Fennel  
267 et al., 2023).

268 Other factors such as temperature or the presence of suitable surfaces for pseudo-homogeneous or heterogeneous precipitation  
269 that were not studied here have an influence on the duration of the nucleation phase and have been suggested as triggers for



270 CaCO<sub>3</sub> precipitation. These suitable surfaces can include but are not limited to fluvial or marine re-suspended particles  
271 (Wurgaft et al., 2021; 2016), seafloor sediments (e.g. CaCO<sub>3</sub>, quartz particles; Moras et al., 2022), small biotic and abiotic  
272 particles (< 50 μm) (Hartmann et al., 2023), seagrass, shells, biofilms, and biological activity (Aloisi et al., 2006, Zhu &  
273 Dittrich, 2016).

274 Dissolving alkaline particles like Ca(OH)<sub>2</sub> or Mg(OH)<sub>2</sub> for OAE could also serve as starting points for carbonate formation  
275 (Moras et al., 2022; Hartmann et al. 2023). When relying on solid alkaline materials, Moras et al. (2022) and Schulz et al.  
276 (2023) suggested that an  $\Omega_{\text{aragonite}}$  of 5 should not be exceeded, above which CaCO<sub>3</sub> runaway precipitation appears to be  
277 triggered. However, under the conditions of this study, i.e., with liquid alkaline material, the  $\Omega_{\text{aragonite}}$  threshold for the initiation  
278 of spontaneous pseudo-homogeneous carbonate formation in particle-free seawater is approximately 11.3 at a salinity of 32.6  
279 and ~11°C (Marion et al., 2009 – based on data from Morse & He, 1993). Most ocean surface waters are naturally oversaturated  
280 with carbonates ( $\Omega_{\text{aragonite}} \sim 2\text{-}5$ , Olsen et al., 2018), yet no obvious spontaneous inorganic carbonate formation is occurring., as  
281 the presence of Mg<sup>2+</sup> (Berner, 1975; Pan et al., 2021), phosphate (Burton & Walter, 1990), and dissolved organic matter species  
282 (Chave & Suess, 1970; Kellock et al., 2022) are known to delay or inhibit precipitation of CaCO<sub>3</sub>. Since Mg<sup>2+</sup> in an open ocean  
283 context correlates to salinity, its concentration could vary depending on the local conditions (Moras et al., 2023), while  
284 phosphate and DOM concentrations are related to biological processes and seasonal changes.

285

#### 286 **4.1.2 Runaway precipitation phase: general patterns**

287 The precipitation phase, characterized by the previously discussed parameters guiding the runaway patterns, might also be  
288 influenced by the concentration and quality of formed particles. In contrast to a natural open ocean environment, where  
289 precipitates could sink and be removed from the alkalinity-enhanced water, the experimental setup here did not take this into  
290 account.

291 It is imperative to investigate if the particle export mechanism could affect the shape of the identified runaway precipitation  
292 patterns, e.g. by lower TA loss rates due to less available suitable surface areas for carbonate formation. The experiments in  
293 this study were performed in bottles, where the presence of precipitation became evident through a fine whitish coating forming  
294 on the inner surface of the water-exposed part of the bottles. Despite being a laboratory artefact, the abundant presence of  
295 suspended particles suggests that in the open ocean, similar precipitation patterns could occur. The observation of crystal  
296 growth on the bottle walls suggests that the results here and the functional relationships of the runaway precipitation might be  
297 impacted by the experimental setup, leading to higher precipitation rates due to increased potential for TA loss. Therefore,  
298 field experiments addressing this issue and confirming or improving the parameterization of the loss functions are  
299 recommended.



300 In natural settings, comparable TA decline patterns were observed in river plumes with high degrees of suspended particles  
301 (Wurgaft et al., 2021; 2016) or whiting events on the Great Bahama Bank (Broecker & Takahashi, 1966; Morse et al., 2003).  
302 One study suggested that with thermohaline stratification and moderate background saturation states in an open water column,  
303 TA loss due to carbonate formation may happen because of strong evaporation of water in the eastern Mediterranean Sea  
304 (Bialik, 2022). The observation that runaway events could occur naturally under certain constrained conditions highlights the  
305 importance of identifying underlying processes before OAE applications are implemented, as the higher saturation states  
306 induced by OAE could make such events likelier.

307 While the fundamental patterns of changes in the carbonate system parameters during the runaway process were dictated by  
308 carbonate formation, the starting and ending points of the procedure were dependent on the initial TA/DIC configuration and  
309 the resulting  $\Omega_{\text{aragonite}}$  achieved through manipulation. The observed differences in TA-loss in CO<sub>2</sub>-equilibrated and non-CO<sub>2</sub>-  
310 equilibrated approaches were therefore expected. Under well-defined circumstances and aware of a practical final  $\Omega_{\text{aragonite}}$   
311 saturation state range, the consequences of a completed runaway precipitation process should, in theory, therefore be  
312 predictable.

313 As shown in Figures 2-4, treatments which underwent a runaway process approached relatively uniform final  $\Omega_{\text{aragonite}}$  values,  
314 indicating that  $\Omega$ -values served as the decisive factor in delineating the termination of the runaway precipitation process.  
315 Including results from this work, runaway precipitation processes in natural or artificial seawater in comparable studies (Moras  
316 et al, 2022; Hartmann et al., 2023; Fuhr et al., 2022; Pan et al., 2021) approached final  $\Omega_{\text{aragonite}}$  values between 1.5 and 5.0.  
317 Variations in the final  $\Omega_{\text{aragonite}}$  in the different approaches might be the result of varying framework conditions during their  
318 runtime.

319

#### 320 **4.1.3 CO<sub>2</sub>-equilibration states**

321

322 While the precipitation rates in this study decreased significantly at the end of each experiment, approaching  $\Omega_{\text{aragonite}}$  values  
323 of 2.5-5.0, it cannot be excluded that further formation of secondary phases could have continued. While some treatments  
324 within the non-CO<sub>2</sub>-equilibrated experiments still experienced a daily decline of 1-10  $\mu\text{eq kgsw}^{-1}$  in TA during the last 5 days  
325 of operation, these changes were relatively insignificant compared to their earlier rates. Nonetheless, slight changes were still  
326 observed, and it cannot be excluded that the process stopped after a runtime of 25 days.

327 In contrast to the CO<sub>2</sub>-non-equilibrated approach, the CO<sub>2</sub>-equilibrated experiments showed relatively constant final  $\Omega_{\text{aragonite}}$   
328 values of 5.8-6.0 at the end of the abiotic experiments after 20 days. The runaway process is anticipated to persist at lower  
329 levels of TA loss rates, given that they consistently declined by 20-30  $\mu\text{eq kgsw}^{-1}$  per day during the final 5 days of operation.

330



#### 331 4.1.4 Comparison to other experiments

332 Time spans to reach the end of the runaway precipitation process in studies with comparable setups, solely focusing on non-  
333 CO<sub>2</sub>-equilibrated treatments with a  $\Delta TA_{\text{added}}$  of 2000  $\mu\text{eq kgsw}^{-1}$ , ranged from 4 days in Hartmann et al. (2023) to more than  
334 14 days in Moras et al. (2022). In Moras et al. (2022), there were variations in the experimental conditions, such as the use of  
335 solid Ca(OH)<sub>2</sub> for TA-enhancement, constant agitation, and a temperature of 21°C. These differences may hinder a direct  
336 comparison with our study. By contrast, this study employed the configuration introduced by Hartmann et al. (2023), with the  
337 only distinction being the utilization of seawater with a salinity of 36.2 and a temperature of around 23°C. In this study, with  
338 a salinity of 32.6 and temperatures ranging from 10 to 16°C, the precipitation process in the highest treatments came close to  
339 a halt after ~15 days in the non-CO<sub>2</sub>-equilibrated approaches, while alkalinity was stable over 20 days in CO<sub>2</sub>-equilibrated  
340 treatments with  $\Delta TA_{\text{added}}$  up to 3600  $\mu\text{eq kgsw}^{-1}$ . However, in Hartmann et al. (2023) experiments, significantly faster  
341 precipitation rates were observed. This underscores the crucial influence of local environmental factors and application  
342 scenario in shaping the dynamics of the runaway process.

343 Following the  $\Omega$ -threshold described by Marion et al. (2009), experimental results from Pytkowicz (1973) and considering the  
344 general trend predictions from the TA-loss rates (Fig. 5), it is suggested that further treatments in this study might have initiated  
345 the runaway process if the experiments had continued. Therefore, treatment levels above  $\Delta TA_{600}$   $\mu\text{eq kgsw}^{-1}$  in the non-CO<sub>2</sub>-  
346 equilibrated and  $\Delta TA_{2400}$   $\mu\text{eq kgsw}^{-1}$  in CO<sub>2</sub>-equilibrated approaches had the potential to start carbonate precipitation.

347 As manipulated water parcels in real world application scenarios would be diluted by untreated water, the results of our study  
348 suggest a functional relationship with time for the dilution of TA-enhanced water to non-critical  $\Omega_{\text{aragonite}}$  values. This could  
349 range from minutes to weeks (e.g. see Figs. 4 and 10), dependent on the local physicochemical conditions, the CO<sub>2</sub>-  
350 equilibration state, and the achieved TA levels. Further research is therefore needed to identify the functional relationship for  
351 other environmental settings such as temperature, salinity, and the impact of particles for near coastal settings. This is necessary  
352 to determine if the here identified relationships are universally valid, or in the context of OAE, further factors need to be  
353 considered. In addition, experiments on the dilution of manipulated water masses are needed to test whether TA values  
354 exceeding critical ranges can be stabilized. By understanding patterns and factors driving the runaway process, measures could  
355 be taken to prevent unwanted consequences during TA addition.

356

#### 357 4.2 Temporal stability after TA addition

358 In the context of an open ocean application of OAE, induced turbulence and advective energy in the water would cause the  
359 mixing of the alkalized water body with untreated surrounding seawater. Specifically, ship-based applications offer the  
360 potential to significantly change the concentrations and saturation states in a relatively short amount of time (e.g. Caserini et





361 al., 2021; He & Tyka, 2023; Renforth & Henderson, 2017). Dilution could potentially prevent or delay the nucleation phase  
362 for a significant amount of time, to a degree that runaway precipitation events can be avoided at time scales relevant for CDR.  
363 While TA values reached in this study might not represent final targeted TA levels for a real-world application after immediate  
364 dilution with untreated water parcels, studied ranges provide experimental insight into processes during transient enhanced  
365 conditions, occurring around point sources or in (partially-) enclosed water bodies without adequate mixing. Derived from the  
366 results of non-CO<sub>2</sub>-equilibrated setups, Fig. 10 provides an overview of TA ranges and timeframes until a manipulated water  
367 mass should be diluted to prevent the onset of secondary mineral formation. Note that for the CO<sub>2</sub>-equilibrated approaches,  
368 this study could not determine reliable comparable stability ranges.

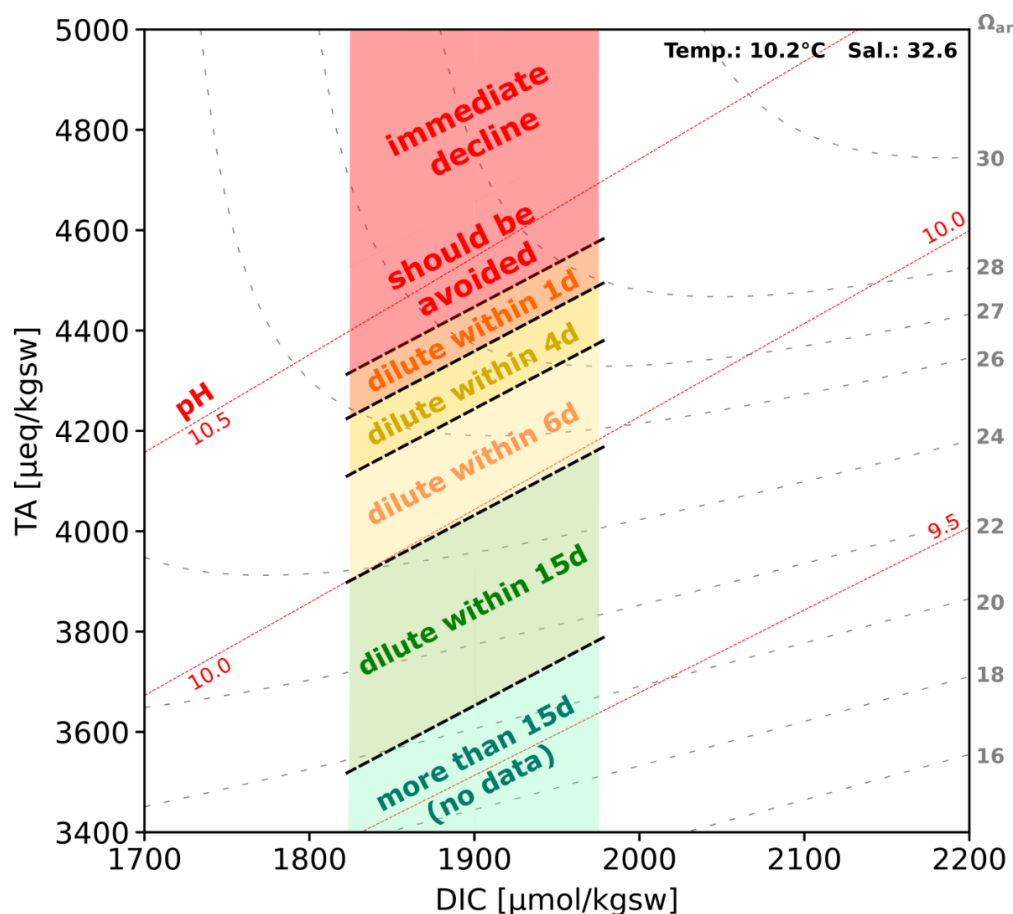


Figure 10: Stability ranges during non-CO<sub>2</sub>-equilibrated experiments showing upper critical limits for application, which should be avoided to prevent runaway precipitation and its consequences.  $\Delta TA_0$  (TA:  $\sim 2200 \mu\text{eq kgsw}^{-1}$ , DIC  $\sim 1900 \mu\text{mol kgsw}^{-1}$ , pH  $\sim 8.2$ , temperature  $10.2^\circ\text{C}$ , salinity  $32.6$ ), the red area highlights the critical zone for immediate precipitation, tolerance in time for dilution or other actions to prevent the runaway process are indicated. Ranges in this diagram are applicable only to this setting and should not be generalized.



369 As described above, treatments which reached TA-levels above  $4450 \mu\text{eq kgsw}^{-1}$  within the non-CO<sub>2</sub>-equilibrated approach  
370 immediately lost parts of the added TA. To avoid any kind of secondary mineral formation under the local conditions of the  
371 Raunefjord, these values should not be surpassed without additional measures. In theory, every ocean water mass should  
372 possess such a critical threshold level for immediate precipitation. This threshold would determine the practical upper limit for  
373 the application scenarios and overall efficiency of OAE. At present, there does not seem to be a comprehensive method for  
374 calculating this upper threshold. Such a method would need to take into consideration the complexities of the natural  
375 environment such as seasonal and biological cycles, distinct geographical characteristics, and the various approaches of TA  
376 addition. To derive such a method would need systematic research to identify relevant factors and field trials aimed at exploring  
377 their interactions under real-world conditions. Nevertheless, results of this study also showed that TA could be enhanced above  
378  $\Delta\text{TA}_{\text{added}}$  of  $2000 \mu\text{eq kgsw}^{-1}$  in a non-CO<sub>2</sub>-equilibrated style without any adverse geochemical consequences if sufficient  
379 mixing is ensured within the given local temporal stability ranges.

#### 380 **4.3 Immediate magnesium hydroxide precipitation**

381 If by addition of NaOH to seawater a pH of 10.4 (at 21 °C) is reached, Mg(OH)<sub>2</sub> is formed. This is a long-known process as  
382 described by Haas (1916) and Kapp (1928) and comparable to values reached in this study within the non-CO<sub>2</sub>-equilibrated  
383 treatments, showing an immediate TA decline (pH 10.3-10.6, at 10-12°C). This suggests that the aforementioned process could  
384 potentially account for the immediate precipitation observed in the present experiments. As described by Turek & Gnot (1995),  
385 the formation of Mg(OH)<sub>2</sub> during this practice could be considered as an “immediate process”, which aligns with observations  
386 in this study. The buffering of TA by Mg(OH)<sub>2</sub> formation during TA injection was also supported by the  $\Delta\text{TA} : \Delta\text{DIC}$  change  
387 ratios of 2.3-4.9:1 (Fig. 4f) immediately after alkalinity addition. Co-precipitation of carbonate phases besides the generation  
388 of Mg(OH)<sub>2</sub> would be necessary to achieve these change ratios and is a regular feature in seawater (Battaglia et al., 2022;  
389 Nguyen Dang et al., 2017; Turek & Gnot, 1995). Formed solid Mg(OH)<sub>2</sub> particles could have acted as triggers for further  
390 precipitation of carbonate phases and leading to the observed earlier initiation of the runaway process.

391 During the injection of NaOH stock solution in seawater, the sharp gradient in pH/TA concentrations could lead to the  
392 generation of lysospheres and floccules, which aggregate and enclose water in its pore space (Turek & Gnot, 1995). Similar  
393 observations were made by Badjatya et al. (2022), who described it as colloidal suspension. While the addition levels were  
394 significantly lower in this study as compared to Badjatya et al. (2022), a comparable trend after the injection was evident. This  
395 trend was visually observable across all non-CO<sub>2</sub>-equilibrated treatments above  $\Delta\text{TA}200$ . However, to observe the same  
396 phenomenon in the CO<sub>2</sub>-equilibrated approaches, higher treatment levels ( $>\Delta\text{TA}2000$ ) were required to form aggregates.  
397 In the absence of further agitation, aggregates that had formed remained visible for several days. However, when the bottles  
398 were gently rotated after the TA addition, aggregates disintegrated and all treatments that were initially below the critical  
399 threshold for immediate precipitation reached their target TA levels. These observations suggest that the immediate formation



400 of potential  $\text{Mg}(\text{OH})_2$  aggregates during the injection process might be reversible, as also noted by Cyronak et al. (2023). In a  
401 real world scenario, wave movement and dilution processes with untreated waters might allow the redissolution of  $\text{Mg}(\text{OH})_2$   
402 or further metastable carbonate phases.

403 Effects like an increase in undesired turbidity during TA addition as stated by Eisaman et al. (2023) might therefore be  
404 temporal. Depending on the speed of the redissolution process, sedimentation of the aggregates might function as an export  
405 factor, transferring the added alkalinity to greater depths. The enclosed water in the lysospheres might nevertheless reduce the  
406 sinking rate significantly due to its relatively low density (Turek & Gnot, 1995).



## 407 5 Conclusion

408

409 After the introduction of the runaway precipitation concept by Moras et al. (2022) and Hartmann et al. (2023), this study has  
410 identified functional relationships of TA change rates after initiation of the secondary carbonate formation process. With well-  
411 defined framework parameters of  $\Omega_{\text{aragonite}}$ , temperature, and salinity, it is therefore possible to predict the temporal evolution  
412 of alkalinity. Once the runaway process was triggered, patterns of TA loss were identical for both CO<sub>2</sub>-equilibrated and non-  
413 CO<sub>2</sub>-equilibrated TA addition approaches. While a progressing runaway process negatively impacts carbonate chemistry  
414 parameters, the observed delayed onset of detectable solid phase formation implies that alkalinity could be enhanced beyond  
415 2000  $\mu\text{eq kgsw}^{-1}$ , when sufficient dilution with untreated water could be ensured within given time ranges. With knowledge  
416 of the local environmental conditions, introduced  $\Omega_{\text{aragonite}}$ , and CO<sub>2</sub>-equilibration state, it is hypothesized that it is possible to  
417 predict a temporary stability range for any given system. The ability to predict the outcomes in advance can facilitate  
418 environmental assessments prior to OAE applications. Furthermore, the parameters acquired could be essential for computer  
419 models to carry out these evaluations.

420 Study results are representative for waters with low suspended sediment concentrations, therefore identified TA rate changes  
421 during runaway precipitation or temporary stability ranges might differ for systems with higher suspended sediment  
422 concentrations, especially if suitable crystal surfaces are abundant (c.f. Moras et al., 2022; Hartmann et al., 2023). Unlike in  
423 Hartmann et al. (2023), no relevant differences between biotic and abiotic approaches (distinguished by the filter mesh size)  
424 could be identified.

425 For non-CO<sub>2</sub>-equilibrated TA additions, an upper pH threshold of around 10.3 could be observed. Crossing this threshold  
426 comes with the potential consequence of magnesium hydroxide formation, which was also seen in other studies (c.f. Badjatya  
427 et al., 2022; Turek & Gnot, 1995; Vassallo et al., 2021). Considerations about the TA-treatment levels in open ocean application  
428 scenarios must therefore consider the onset of Mg(OH)<sub>2</sub> formation as an upper threshold. To maximize effectiveness, it is  
429 crucial to maintain concentrations just below this critical value when injecting alkalinity into seawater, especially if the local  
430 seawater possess efficient dilution capabilities.

431 These considerations are relevant for modelling the limitations and dynamics of alkalinity enhancement in the ocean, as  
432 demonstrated by He and Tyka (2023). Nevertheless, it is essential to validate these findings with in situ experiments to establish  
433 parameters and functional relationships applicable to open ocean environments. It is only under these circumstances that  
434 accurate assessments can be made. The most promising outcome of this study is the possibility to predict abiotic processes and  
435 the stability of alkalinity for effective and realistic applications in the future.



436 **Author contributions**

437

438 The idea for this work was conceived by NS and JH. NS, GF, and CL designed the experiments with help from JH, JS, and  
439 UR. NS, CL, GF, and JS carried out sampling and laboratory analysis. NS interpreted the data with help from GF and JH. NS  
440 and JH wrote the text with contributions from all co-authors.

441

442 **Acknowledgements**

443

444 Peggy Bartsch (UHH), Tom Jäppinen (UHH), and Daniel Brüggemann (GEOMAR) are thanked for supporting the preparation  
445 and execution of the experiments. This project has received funding from the European Union’s Horizon 2020 research and  
446 innovation program under grant agreement no. 869357 (project OceanNETs, ocean-based negative emission technologies –  
447 analyzing the feasibility, risks, and co-benefits of ocean-based negative emission technologies for stabilizing the climate), as  
448 well as the Deutsche Forschungsgemeinschaft (DFG, German Research Foundation) under Germany’s Excellence Strategy –  
449 EXC 2037 “CLICCS – Climate, Climatic Change, and Society” – Project Number: 390683824, contribution to the Center for  
450 Earth System Research and Sustainability (CEN) of Universität Hamburg. Financial support was also provided by the Ocean  
451 Alkalinity Enhancement (OAE) R&D Program, a multi-funder effort incubated by Carbon to Sea Initiative via the Ocean Alk-  
452 align-project.

453

454 **Financial support**

455 This research has been supported by the Horizon 2020 (OceanNETs (grant no. 869357)), the Deutsche  
456 Forschungsgemeinschaft (grant no. 390683824) and the Ocean Alkalinity Enhancement (OAE) R&D Program funded by the  
457 Carbon to Sea Initiative.

458

459 **Competing interests**

460 JHA is a co-founder of the Planeteeers GmbH. The contact author has declared that all other authors have no competing interests.



## 461 References

- 462 Albright, R., Caldeira, L., Hosfelt, J., Kwiatkowski, L., Maclaren, J. K., Mason, B. M., Nebuchina, Y., Ninokawa, A., Pongratz,  
463 J., Ricke, K. L., Rivlin, T., Schneider, K., Sesboüé, M., Shamberger, K., Silverman, J., Wolfe, K., Zhu, K., and  
464 Caldeira, K.: Reversal of ocean acidification enhances net coral reef calcification, *Nature*, 531, 362–365,  
465 <https://doi.org/10.1038/nature17155>, 2016.
- 466 Aloisi, G., Gloter, A., Krüger, M., Wallmann, K., Guyot, F., and Zuddas, P.: Nucleation of calcium carbonate on bacterial  
467 nanoglobules, *Geology*, 34, <https://doi.org/10.1130/g22986a.1>, 2006.
- 468 Bach, L. T., Gill, S. J., Rickaby, R. E. M., Gore, S., and Renforth, P.: CO<sub>2</sub> Removal With Enhanced Weathering and Ocean  
469 Alkalinity Enhancement: Potential Risks and Co-benefits for Marine Pelagic Ecosystems, *Frontiers in Climate*, 1,  
470 1038, <https://doi.org/10.3389/fclim.2019.00007>, 2019.
- 471 Badjatya, P., Akca, A. H., Fraga Alvarez, D. V., Chang, B., Ma, S., Pang, X., Wang, E., van Hinsberg, Q., Esposito, D. V.,  
472 and Kawashima, S.: Carbon-negative cement manufacturing from seawater-derived magnesium feedstocks, *Proc Natl*  
473 *Acad Sci U S A*, 119, e2114680119, <https://doi.org/10.1073/pnas.2114680119>, 2022.
- 474 Badocco, D., Pedrini, F., Pastore, A., di Marco, V., Marin, M. G., Bogianni, S., Roverso, M., and Pastore, P.: Use of a simple  
475 empirical model for the accurate conversion of the seawater pH value measured with NIST calibration into seawater  
476 pH scales, *Talanta*, 225, 122051, <https://doi.org/10.1016/j.talanta.2020.122051>, 2021.
- 477 Battaglia, G., Domina, M. A., Lo Brutto, R., Lopez Rodriguez, J., Fernandez de Labastida, M., Cortina, J. L., Pettignano, A.,  
478 Cipollina, A., Tamburini, A., and Micale, G.: Evaluation of the Purity of Magnesium Hydroxide Recovered from  
479 Saltwork Bitterns, *Water*, 15, <https://doi.org/10.3390/w15010029>, 2022.
- 480 Berner, R. A.: The role of magnesium in the crystal growth of calcite and aragonite from sea water, *Geochimica et*  
481 *Cosmochimica Acta*, 39, 489-504, [https://doi.org/10.1016/0016-7037\(75\)90102-7](https://doi.org/10.1016/0016-7037(75)90102-7), 1975.
- 482 Berner, R. A., Lasaga, A. C., and Garrels, R. M.: Carbonate-silicate geochemical cycle and its effect on atmospheric carbon  
483 dioxide over the past 100 million years, *Am. J. Sci.:(United States)*, 283, <https://doi.org/10.2475/ajs.283.7.641>, 1983.
- 484 Bialik, O. M., Sisma-Ventura, G., Vogt-Vincent, N., Silverman, J., and Katz, T.: Role of oceanic abiotic carbonate precipitation  
485 in future atmospheric CO<sub>2</sub> regulation, *Sci Rep*, 12, 15970, <https://doi.org/10.1038/s41598-022-20446-7>, 2022.
- 486 Boon, M., Rickard, W. D. A., Rohl, A. L., and Jones, F.: Stabilization of Aragonite: Role of Mg<sup>2+</sup> and Other Impurity Ions,  
487 *Crystal Growth & Design*, 20, 5006-5017, <https://doi.org/10.1021/acs.cgd.0c00152>, 2020.
- 488 Broecker, W. S. and Takahashi, T.: Calcium carbonate precipitation on the Bahama Banks, *Journal of Geophysical Research*,  
489 71, 1575-1602, <https://doi.org/10.1029/JZ071i006p01575>, 1966.
- 490 Burton, E. A. and Walter, L. M.: The role of pH in phosphate inhibition of calcite and aragonite precipitation rates in seawater,  
491 *Geochimica et Cosmochimica Acta*, 54, 797-808, [https://doi.org/10.1016/0016-7037\(90\)90374-T](https://doi.org/10.1016/0016-7037(90)90374-T), 1990.



- 492 Caldeira, K. and Rau, G. H.: Accelerating carbonate dissolution to sequester carbon dioxide in the ocean: Geochemical  
493 implications, *Geophysical Research Letters*, 27, 225-228, <https://doi.org/10.1029/1999gl002364>, 2000.
- 494 Caserini, S., Pagano, D., Campo, F., Abbà, A., De Marco, S., Righi, D., Renforth, P., and Grosso, M.: Potential of Maritime  
495 Transport for Ocean Liming and Atmospheric CO<sub>2</sub> Removal, *Frontiers in Climate*, 3,  
496 <https://doi.org/10.3389/fclim.2021.575900>, 2021.
- 497 Chave, K. E. and Suess, E.: Calcium Carbonate Saturation in Seawater: Effects of Dissolved Organic Matter, *Limnology and  
498 Oceanography*, 15, 633-637, <https://doi.org/10.4319/lo.1970.15.4.0633>, 1970.
- 499 Cyronak, T., Albright, R., and Bach, L.: Chapter 4.5: Field Experiments, *State of the Planet Discussions*, 2023, 1-25,  
500 <https://doi.org/10.5194/sp-2023-9>, 2023.
- 501 Deffeyes, K. S.: Carbonate Equilibria: A Graphic and Algebraic Approach<sup>1</sup>, *Limnology and Oceanography*, 10, 412-426,  
502 <https://doi.org/10.4319/lo.1965.10.3.0412>, 1965.
- 503 Dickson, A. G.: Standard potential of the reaction: AgCl(s) + 1/2 H<sub>2</sub>(g) = Ag(s) + HCl(aq), and the standard acidity constant  
504 of the ion HSO<sub>4</sub><sup>-</sup> in synthetic sea water from 273.15 to 318.15 K, *The Journal of Chemical Thermodynamics*, 22,  
505 113-127, [https://doi.org/10.1016/0021-9614\(90\)90074-Z](https://doi.org/10.1016/0021-9614(90)90074-Z), 1990.
- 506 Eisaman, M., Geilert, S., Renforth, P., Bastianini, L., Campbell, J., Dale, A., Foteinis, S., Grasse, P., Hawrot, O., and Löscher,  
507 C.: Chapter 3: Assessing the technical aspects of OAE approaches, *State of the Planet Discussions*, 2023, 1-52,  
508 <https://doi.org/10.5194/sp-2-oae2023-3-2023>, 2023.
- 509 Fennel, K., Long, M. C., Algar, C., Carter, B., Keller, D., Laurent, A., Mattern, J. P., Musgrave, R., Oschlies, A., and Ostiguy,  
510 J.: Modeling considerations for research on Ocean Alkalinity Enhancement (OAE), *State of the Planet Discussions*,  
511 2023, 1-47, <https://doi.org/10.5194/sp-2-oae2023-9-2023>, 2023.
- 512 Ferderer, A., Chase, Z., Kennedy, F., Schulz, K. G., and Bach, L. T.: Assessing the influence of ocean alkalinity enhancement  
513 on a coastal phytoplankton community, *Biogeosciences*, 19, 5375-5399, [10.5194/bg-19-5375-2022](https://doi.org/10.5194/bg-19-5375-2022), 2022.
- 514 Forster, M.: Investigations for the environmentally friendly production of Na<sub>2</sub>CO<sub>3</sub> and HCl from exhaust CO<sub>2</sub>, NaCl and  
515 H<sub>2</sub>O, *Journal of Cleaner Production*, 23, 195-208, <https://doi.org/10.1016/j.jclepro.2011.10.012>, 2012.
- 516 Forster, M.: Investigations to convert CO<sub>2</sub>, NaCl and H<sub>2</sub>O into Na<sub>2</sub>CO<sub>3</sub> and HCl by thermal solar energy with high solar  
517 efficiency, *Journal of CO<sub>2</sub> Utilization*, 7, 11-18, <https://doi.org/10.1016/j.jcou.2014.06.001>, 2014.
- 518 Fuhr, M., Geilert, S., Schmidt, M., Liebetrau, V., Vogt, C., Ledwig, B., and Wallmann, K.: Kinetics of Olivine Weathering in  
519 Seawater: An Experimental Study, *Frontiers in Climate*, 4, <https://doi.org/10.3389/fclim.2022.831587>, 2022.
- 520 Haas, A. R.: The Effect of the Addition of Alkali to Sea Water Upon the Hydrogen Ion Concentration, *Journal of Biological  
521 Chemistry*, 26, 515-517, [https://doi.org/10.1016/s0021-9258\(18\)87433-6](https://doi.org/10.1016/s0021-9258(18)87433-6), 1916.
- 522 Hartmann, J., West, A. J., Renforth, P., Köhler, P., De La Rocha, C. L., Wolf-Gladrow, D. A., Dürr, H. H., and Scheffran, J.:  
523 Enhanced chemical weathering as a geoengineering strategy to reduce atmospheric carbon dioxide, supply nutrients,  
524 and mitigate ocean acidification, *Reviews of Geophysics*, 51, 113-149, <https://doi.org/10.1002/rog.20004>, 2013.



- 525 Hartmann, J., Suitner, N., Lim, C., Schneider, J., Marín-Samper, L., Arístegui, J., Renforth, P., Taucher, J., and Riebesell, U.:  
526 Stability of alkalinity in ocean alkalinity enhancement (OAE) approaches – consequences for durability of CO<sub>2</sub>  
527 storage, *Biogeosciences*, 20, 781–802, <https://doi.org/10.5194/bg-20-781-2023>, 2023.
- 528 He, J. and Tyka, M. D.: Limits and CO<sub>2</sub> equilibration of near-coast alkalinity enhancement, *Biogeosciences*, 20, 27–43,  
529 <https://doi.org/10.5194/bg-20-27-2023>, 2023.
- 530 Ilyina, T., Six, K. D., Segschneider, J., Maier-Reimer, E., Li, H., and Núñez-Riboni, I.: Global ocean biogeochemistry model  
531 HAMOCC: Model architecture and performance as component of the MPI-Earth system model in different CMIP5  
532 experimental realizations, *Journal of Advances in Modeling Earth Systems*, 5, 287–315,  
533 <https://doi.org/10.1029/2012ms000178>, 2013.
- 534 Kapp, E. M.: The precipitation of calcium and magnesium from sea water by sodium hydroxide, *The Biological Bulletin*, 55,  
535 453–458, 1928.
- 536 Kellock, C., Castillo Alvarez, M. C., Finch, A., Penkman, K., Kroger, R., Clog, M., and Allison, N.: Optimising a method for  
537 aragonite precipitation in simulated biogenic calcification media, *PLoS One*, 17, e0278627,  
538 <https://doi.org/10.1371/journal.pone.0278627>, 2022.
- 539 Kheshgi, H. S.: Sequestering atmospheric carbon dioxide by increasing ocean alkalinity, *Energy*, 20(9), 915–922.,  
540 [https://doi.org/10.1016/0360-5442\(95\)00035-F](https://doi.org/10.1016/0360-5442(95)00035-F) 1995.
- 541 Koch, C. and Manzur, K.: A new technology of pit lake treatment using calcium oxide and carbon dioxide to increase alkalinity,  
542 IMWA 2016 – Mining Meets Water – Conflicts and Solutions, International Mine Water Association, 284–229, 2016.
- 543 Köhler, P., Hartmann, J., and Wolf-Gladrow, D. A.: Geoengineering potential of artificially enhanced silicate weathering of  
544 olivine, *Proc Natl Acad Sci U S A*, 107, 20228–20233, <https://doi.org/10.1073/pnas.1000545107>, 2010.
- 545 Lee, K., Kim, T.-W., Byrne, R. H., Millero, F. J., Feely, R. A., and Liu, Y.-M.: The universal ratio of boron to chlorinity for  
546 the North Pacific and North Atlantic oceans, *Geochimica et Cosmochimica Acta*, 74, 1801–1811,  
547 <https://doi.org/10.1016/j.gca.2009.12.027>, 2010.
- 548 LMBV: In-lake Neutralization of East German Lignite Pit Lakes: Technical History and New Approaches from LMBV, 2017.
- 549 Lueker, T. J., Dickson, A. G., and Keeling, C. D.: Ocean pCO<sub>2</sub> calculated from dissolved inorganic carbon, alkalinity, and  
550 equations for K<sub>1</sub> and K<sub>2</sub>: validation based on laboratory measurements of CO<sub>2</sub> in gas and seawater at equilibrium,  
551 *Marine chemistry*, 70(1–3), 105–119, [https://doi.org/10.1016/S0304-4203\(00\)00022-0](https://doi.org/10.1016/S0304-4203(00)00022-0), 2000.
- 552 Mackenzie, F. T. and Garrels, R. M.: Chemical mass balance between rivers and oceans, *American Journal of Science*, 264,  
553 507–525, <https://doi.org/10.2475/ajs.264.7.507>, 1966.
- 554 Marion, G., Millero, F., and Feistel, R.: Precipitation of solid phase calcium carbonates and their effect on application of  
555 seawater S A–T–P models, *Ocean science*, 5, 285–291, <https://doi.org/10.5194/os-5-285-2009>, 2009.
- 556 Meinshausen, M., Meinshausen, N., Hare, W., Raper, S. C., Frieler, K., Knutti, R., Frame, D. J., and Allen, M. R.: Greenhouse-  
557 gas emission targets for limiting global warming to 2 degrees C, *Nature*, 458, 1158–1162,  
558 <https://doi.org/10.1038/nature08017>, 2009.





- 559 Moras, C., Bach, L., Cyronak, T., Joannes-Boyau, R., and Schulz, K.: Effects of grain size and seawater salinity on brucite  
560 dissolution and secondary calcium carbonate precipitation kinetics: implications for Ocean Alkalinity Enhancement,  
561 Copernicus Meetings, <https://doi.org/10.5194/egusphere-egu23-330>, 2023.
- 562 Moras, C. A., Bach, L. T., Cyronak, T., Joannes-Boyau, R., and Schulz, K. G.: Ocean alkalinity enhancement – avoiding  
563 runaway CaCO<sub>3</sub> precipitation during quick and hydrated lime dissolution, *Biogeosciences*, 19, 3537-3557,  
564 <https://doi.org/10.5194/bg-19-3537-2022>, 2022.
- 565 Morse, J. W. and He, S.: Influences of T, S and PCO<sub>2</sub> on the pseudo-homogeneous precipitation of CaCO<sub>3</sub> from seawater:  
566 implications for whiting formation, *Marine Chemistry*, 41(4), 291-297., [https://doi.org/10.1016/0304-](https://doi.org/10.1016/0304-4203(93)90261-L)  
567 [4203\(93\)90261-L](https://doi.org/10.1016/0304-4203(93)90261-L), 1993.
- 568 Morse, J. W., Arvidson, R. S., and Lüttge, A.: Calcium carbonate formation and dissolution, *Chemical reviews*, 107, 342-381,  
569 <https://doi.org/10.1021/cr050358j>, 2007.
- 570 Morse, J. W., Gledhill, D. K., and Millero, F. J.: CaCO<sub>3</sub> precipitation kinetics in waters from the great Bahama bank,  
571 *Geochimica et Cosmochimica Acta*, 67, 2819-2826, [https://doi.org/10.1016/s0016-7037\(03\)00103-0](https://doi.org/10.1016/s0016-7037(03)00103-0), 2003.
- 572 Morse, J. W., Wang, Q., and Tsio, M. Y.: Influences of temperature and Mg: Ca ratio on CaCO<sub>3</sub> precipitates from seawater,  
573 *Geology*, 25, 85-87, [https://doi.org/10.1130/0091-7613\(1997\)025<0085:IOTAMC>2.3.CO;2](https://doi.org/10.1130/0091-7613(1997)025<0085:IOTAMC>2.3.CO;2), 1997.
- 574 NASEM: A Research Strategy for Ocean-based Carbon Dioxide Removal and Sequestration, National Academies of Sciences,  
575 Engineering, and Medicine, Washington (DC), <https://doi.org/10.17226/26278>, 2022.
- 576 Nguyen Dang, D., Gascoïn, S., Zanibellato, A., G. Da Silva, C., Lemoine, M., Riffault, B., Sabot, R., Jeannin, M., Chateigner,  
577 D., and Gil, O.: Role of brucite dissolution in calcium carbonate precipitation from artificial and natural seawaters,  
578 *Crystal Growth & Design*, 17, 1502-1513, <https://doi.org/10.1021/acs.cgd.6b01305>, 2017.
- 579 Nielsen, M. H., Aloni, S., and De Yoreo, J. J.: In situ TEM imaging of CaCO<sub>3</sub> nucleation reveals coexistence of direct and  
580 indirect pathways, *Science*, 345, 1158-1162, <https://doi.org/10.1126/science.1254051>, 2014.
- 581 Olsen, A., Lange, N., Key, R. M., Tanhua, T., Álvarez, M., Becker, S., Bittig, H. C., Carter, B. R., Cotrim da Cunha, L., and  
582 Feely, R. A.: GLODAPv2. 2019—an update of GLODAPv2, *Earth System Science Data*, 11, 1437-1461,  
583 <https://doi.org/10.5194/essd-11-1437-2019>, 2019.
- 584 Orr, J. C., Epitalon, J.-M., Dickson, A. G., and Gattuso, J.-P.: Routine uncertainty propagation for the marine carbon dioxide  
585 system, *Marine Chemistry*, 207, 84-107, <https://doi.org/10.1016/j.marchem.2018.10.006>, 2018.
- 586 Pan, Y., Li, Y., Ma, Q., He, H., Wang, S., Sun, Z., Cai, W.-J., Dong, B., Di, Y., Fu, W., and Chen, C.-T. A.: The role of Mg<sup>2+</sup>  
587 in inhibiting CaCO<sub>3</sub> precipitation from seawater, *Marine Chemistry*, 237,  
588 <https://doi.org/10.1016/j.marchem.2021.104036>, 2021.
- 589 Paul, A., Haunost, M., Goldenberg, S., Sanchez Smith, N., and Riebesell, U.: Testing the response of natural plankton  
590 community to ocean alkalinity enhancement in the subtropical North Atlantic Ocean,  
591 <https://doi.org/10.5194/egusphere-egu23-9528>, 2023.



- 592 Pierrot, D., Lewis, E., and Wallace, D. W. R.: MS Excel Program Developed for CO<sub>2</sub> System Calculations ORNL/CDIAC-  
593 105a (Co2sys\_v2.5) [code], 10.3334/CDIAC/otg.CO2SYS\_XLS\_CDIAC105a, 2006.
- 594 Pytkowicz, R.: Calcium carbonate retention in supersaturated seawater, American Journal of Science, 273, 515-522,  
595 <http://dx.doi.org/10.2475/ajs.273.6.515> 1973.
- 596 Renforth, P. and Henderson, G.: Assessing ocean alkalinity for carbon sequestration, Reviews of Geophysics, 55, 636-674,  
597 <https://doi.org/10.1002/2016rg000533>, 2017.
- 598 Riebesell, U., Basso, D., Geilert, S., Dale, A. W., Kreuzburg, M., and Meysman, F.: Mesocosm experiments in ocean alkalinity  
599 enhancement research, State of the Planet Discussions, 2023, 1-21, <https://doi.org/10.5194/sp-2-oae2023-6-2023>,  
600 2023.
- 601 Rogelj, J., Schaeffer, M., Friedlingstein, P., Gillett, N. P., van Vuuren, D. P., Riahi, K., Allen, M., and Knutti, R.: Differences  
602 between carbon budget estimates unravelled, Nature Climate Change, 6, 245-252,  
603 <https://doi.org/10.1038/nclimate2868>, 2016.
- 604 Sánchez, N., Goldenberg, S. U., Brüggemann, D., Weichler, M., Dorssers, S., and Riebesell, U.: Ecosystem impacts of Ocean  
605 Alkalinization in an oligotrophic marine plankton community: A mesocosm study, Copernicus Meetings,  
606 <https://doi.org/10.5194/egusphere-egu23-15436>, 2023.
- 607 Schuiling, R. D. and Krijgsman, P.: Enhanced Weathering: An Effective and Cheap Tool to Sequester Co<sub>2</sub>, Climatic Change,  
608 74, 349-354, <https://doi.org/10.1007/s10584-005-3485-y>, 2006.
- 609 Schulz, K. G., Bach, L. T., and Dickson, A. G.: Seawater carbonate system considerations for ocean alkalinity enhancement  
610 research, State of the Planet Discussions, 2023, 1-24, <https://doi.org/10.5194/sp-2-oae2023-2-2023>, 2023.
- 611 Sterling, S., Halfyard, E., Hart, K., Trueman, B., Grill, G., and Lehner, B.: Addition of Alkalinity to Rivers: a new CO<sub>2</sub>  
612 Removal Strategy, ESS Open Archive, <https://doi.org/10.22541/essoar.168380809.92137625/v1>, 2023.
- 613 Turek, M. and Gnot, W.: Precipitation of magnesium hydroxide from brine, Industrial & engineering chemistry research, 34,  
614 244-250, <https://doi.org/10.1021/ie00040a025>, 1995.
- 615 UNFCCC: Report of the Conference of the Parties to the United Nations Framework Convention on Climate Change (21st  
616 Session, 2015: Paris). Retrived December. Vol. 4. 2015., 2015.
- 617 Vassallo, F., La Corte, D., Cancilla, N., Tamburini, A., Bevacqua, M., Cipollina, A., and Micale, G.: A pilot-plant for the  
618 selective recovery of magnesium and calcium from waste brines, Desalination, 517,  
619 <https://doi.org/10.1016/j.desal.2021.115231>, 2021.
- 620 Wurgaft, E., Steiner, Z., Luz, B., and Lazar, B.: Evidence for inorganic precipitation of CaCO<sub>3</sub> on suspended solids in the  
621 open water of the Red Sea, Marine Chemistry, 186, 145-155, <https://doi.org/10.1016/j.marchem.2016.09.006>, 2016.
- 622 Wurgaft, E., Wang, Z. A., Churchill, J. H., Dellapenna, T., Song, S., Du, J., Ringham, M. C., Rivlin, T., and Lazar, B.: Particle  
623 Triggered Reactions as an Important Mechanism of Alkalinity and Inorganic Carbon Removal in River Plumes,  
624 Geophysical Research Letters, 48, 277, <https://doi.org/10.1029/2021gl093178>, 2021.



- 625 Yang, B., Leonard, J., and Langdon, C.: Seawater alkalinity enhancement with magnesium hydroxide and its implication for  
626 carbon dioxide removal, *Marine chemistry*, <https://doi.org/10.1016/j.marchem.2023.104251>, 2023.
- 627 Zeebe, R. and Wolf-Gladrow, D.: *CO<sub>2</sub> in Seawater: Equilibrium, Kinetics, Isotopes*, Elsevier Oceanography Book Series. 65,  
628 Amsterdam, 361 pp.2001.
- 629 Zhu, T. and Dittrich, M.: Carbonate Precipitation through Microbial Activities in Natural Environment, and Their Potential in  
630 Biotechnology: A Review, *Front Bioeng Biotechnol*, 4, 4, <https://doi.org/10.3389/fbioe.2016.00004>, 2016.

631